Materials Today 88 (2025) 1005–1027

Contents lists available at ScienceDirect

Materials Today

journal homepage: www.elsevier.com/locate/mattod

Research

Development of advanced anodes for solid-state lithium batteries

Zhenqi Song [a], Yanjiao Ma [b,*], Xinbing Cheng [a], Zhi Zhu [a], Yiren Zhong [a], Jiarui He [a], Tao Wang [a], Dinghao Xu [c], Qianyu Zhang [c,*], Kenneth I. Ozoemena [d], Torsten Brezesinski [e,*], Yuan Ma [a,*], Stefano Passerini [f], Yuping Wu [a,*]

[a] Confucius Energy Storage Lab, Key Laboratory of Energy Thermal Conversion and Control of Ministry of Education, School of Energy and Environment & Z Energy Storage Center, Southeast University, Nanjing 211189, China
[b] School of Energy and Mechanical Engineering, Nanjing Normal University, Nanjing 210023, China
[c] College of Materials Science and Engineering, Sichuan University, Chengdu 610064, China
[d] Molecular Sciences Institute, School of Chemistry, University of the Witwatersrand, Johannesburg, South Africa
[e] Institute of Nanotechnology, Karlsruhe Institute of Technology (KIT), Kaiserstr. 12, 76131 Karlsruhe, Germany
[f] Austrian Institute of Technology (AIT) Center for Transportation Technologies, Giefinggasse 4, 1220 Wien, Austria

ARTICLE INFO

Keywords:
Solid-state batteries
Anode active materials
Anode design
Optimization strategies
Superionic solid electrolytes

ABSTRACT

Solid-state batteries (SSBs) may offer superior energy density, faster charging kinetics, better safety, and extended lifespan compared to conventional lithium-ion batteries that utilize flammable liquid electrolytes. These advantages position SSBs as a leading candidate for next-generation energy storage technologies, particularly in applications requiring high efficiency and safety, such as electric vehicles and renewable energy systems. At the core of SSB technology is the anode active material (AAM), which plays a crucial role in determining the battery's energy density, cycling stability, and overall safety. This review systematically summarizes various AAMs employed in solid-state environments, encompassing a diverse range of materials, including metal-, carbon-, and alloy-based systems. Furthermore, it examines recent advancements in AAM design, focusing on innovative optimization strategies that enhance battery performance. By providing a thorough analysis of these materials and the progress made in their development, this review offers valuable insights into the future trends, opportunities, and challenges in the field of high-performance SSBs.

Introduction

With the steady expansion of the electric vehicle market, secondary battery technology, namely, lithium-ion batteries (LIBs), is progressing towards higher energy and power densities [1,2]. Nevertheless, this progress in technology frequently accompanies thermodynamic instability, which has sparked increasing apprehension among consumers about the safety of mobile devices [3,4]. The main cause of battery thermal failure is the utilization of flammable organic electrolytes, which present hazards of leakage and fire [5,6]. Constructing solid-state batteries (SSBs) with superionic solid electrolytes (SEs) offers a promising solution, as these materials not only enhance safety but also contribute to improved cell-level energy density [7–9]. SSBs hold strong application potential and are being actively developed globally, driven by national policies and strategic plans [10,11]. In the United States, SSBs are viewed as essential for maintaining leadership in battery technology, with the "National Lithium Battery Blueprint for 2021 – 2030" highlighting them as a key objective. The European Battery Alliance's "BATTERY 2030 + Roadmap" emphasizes SSBs' potential in self-healing and intelligent battery systems. In 1987, China included SSBs in the "863" Program, and their strategic role was further reinforced by the 2020 "New Energy Vehicle Industry Development Plan (2021–2035)." The Society of Automotive Engineers of China's "Roadmap 2.0" sets ambitious performance targets for high-energy–density batteries, namely 350 Wh kg^{-1} by 2025, 400 Wh kg^{-1} by 2030, and over 500 Wh kg^{-1} by 2035. These targets outline an ambitious vision for the future, focusing on enhancing energy density, safety, and long-term stability, which are crucial for the widespread adoption of SSBs [12].

Amidst this backdrop, companies in the industrial sector are actively working to translate these technological advancements into commercially viable solutions, paving the way for a new era in sustainable transportation. Notably, Solid Power has been dedicated to the

* Corresponding authors.
E-mail addresses: yanjiao.ma@njnu.edu.cn (Y. Ma), zhangqianyu@scu.edu.cn (Q. Zhang), torsten.brezesinski@kit.edu (T. Brezesinski), yuan.ma@seu.edu.cn (Y. Ma), wuyp@fudan.edu.cn (Y. Wu).

https://doi.org/10.1016/j.mattod.2025.06.041
Received 16 February 2025; Received in revised form 20 April 2025; Accepted 26 June 2025
Available online 11 July 2025
1369-7021/© 2025 Elsevier Ltd. All rights are reserved, including those for text and data mining, AI training, and similar technologies.

development and mass production of SSBs. Its battery design, featuring a "lithium nickel cobalt manganese oxide (NCM or NMC) cathode + SE + lithium metal anode," can achieve an energy density of 440 Wh kg^{-1}. In terms of industrialization, Solid Power established a 1 MWh pilot production line in June 2022, which is compatible with traditional LIB production lines, enabling quick transition towards GWh-scale mass production. Currently, Solid Power produces batteries using a design of "50 % silicon anode + SE + NCM cathode," with a weekly output of approximately 300 units and an annual output of around 15,000 units, aiming to begin full-scale production in 2026 [13].

In academia, research on SSBs has surged, with publications increasing in number significantly since 2010, as illustrated in the bar chart in Fig. 1. The majority of these studies focus on SEs, highlighting their critical role in advancing SSB technology. Nevertheless, SSBs remain in the early stages of development, and progress in SEs alone will not be sufficient to guarantee major enhancements in performance. Equally crucial is the advancement of electrode active materials having energy densities that meet or exceed those of current LIBs. These materials need to possess both high specific capacities and demonstrate robust chemical and electrochemical stability, as well as good compatibility with SEs to ensure stable cycling of SSBs [6,14,15].

Anode active materials (AAMs) are crucial components in advanced SSBs (Fig. 2) since they must provide high performance, including high specific capacity, excellent stability, and fast ion and electron transport capabilities [6,16]. These attributes are essential for ensuring the effective and steady operation of the battery. Among various AAMs, lithium metal anodes have garnered significant interest in the development of SSB technology, primarily due to their high theoretical specific capacity of 3860 mAh g^{-1} and low electrochemical potential [−3.04 V vs. standard hydrogen electrode (SHE)] [17,18]. Nevertheless, in practical applications, the use of lithium metal anodes often results in unstable interfaces with SEs due to significant volume changes (chemo-mechanical degradation) and undesirable side reactions. These issues make lithium metal anodes highly susceptible to loss of electrochemically active material and dendrite growth [19,20]. The latter not only causes damage to the structure of SSBs but also has the potential to rupture the SE (which may also act as separator), posing significant risks to the safety and lifespan of the battery [21,22]. The structure and composition of lithium metal anodes directly affect the deposition and dissolution behavior of lithium ions. By carefully designing the intrinsic structure and optimizing its composition, fast ion transport can be achieved, mitigating side reactions with the SEs, maintaining interface stability, and inhibiting the growth of lithium dendrites [23,24]. In addition to lithium metal, alloys, and carbon-based materials are also promising AAMs due to their beneficial properties [25]. Among them, alloys can provide specific capacities comparable to that of the lithium metal anode, but importantly, they are capable of mitigating the electrode breathing to some extent, thereby significantly extending the battery's cycle life [26]. Carbon-based AAMs such as graphite, hard carbon (HC), soft carbon, carbon nanotubes, etc. offer a rigid structure and unique lithium-ion storage mechanisms (primarily of insertion type), limiting volume changes upon lithiation to less than 10 % [27]. Furthermore, these materials are typically of high electronic conductivity and exhibit good chemical stability, both of which contribute positively to the overall performance of SSBs [28]. Notably, the recent development of anode-less SSBs represents a significant breakthrough, enhancing energy density by reducing the mass of inactive materials on the negative electrode side [29,30].

As scientific research advances and technology progresses, numerous new types of AAMs are being developed. These materials are finding increasing use in advanced SSBs, leading to substantial improvements in performance and rapid growth of the field [31]. Recent years have seen a notable increase in publications related to anode active materials, reflecting the growing interest in this area. Although several summaries have emerged for lithium metal, recent studies highlight the potential of alloy- and carbon-based anodes in SSBs, necessitating a comparative analysis to reveal future development trends. This study establishes the first unified framework integrating lithium metal as well as carbon- and alloy-based AAMs, systematically elucidating the distinct characteristics of these materials in SSB applications. Through multidimensional comparative analysis, we reveal that while lithium metal offers theoretical capacity advantages, it faces engineering bottlenecks, whereas carbonaceous anodes demonstrate excellent cost-effectiveness due to mature manufacturing processes, and alloy-based AAMs exhibit high-capacity prospects through structural design innovations. Specifically, dendrite challenges need to be overcome in the case of lithium metal to achieve high energy densities; the compatibility of carbon-type AAMs needs to be enhanced through, e.g., composite modifications; and alloy-based AAMs require solutions to issues relating to volume variations for high-capacity applications. Notably, these materials are not simply substitutable alternatives, but rather their synergistic development relies on advancements in SE design/chemistry and device integration technologies. We anticipate that this study will also offer useful perspectives for researchers in related disciplines and contribute to the continuous advancement of anode technologies in SSBs.

Solid-state battery anode active materials

The properties of AAMs play a crucial role in determining the overall performance of SSBs, affecting factors such as energy density, efficiency, lifespan, and safety. AAMs that are considered ideal must exhibit stable physicochemical properties and demonstrate promising electrochemical

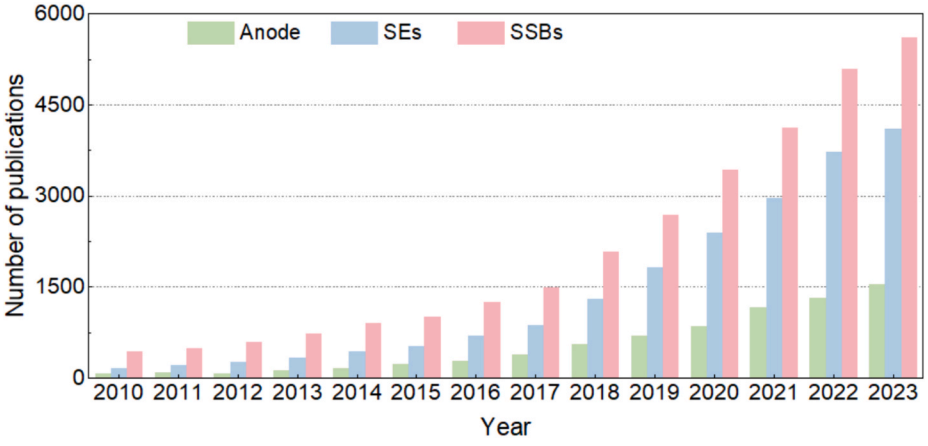

Fig. 1. Number of papers published on SEs and anodes for application in SSBs (Web of Science, combined search for "all-solid-state batteries", "solid-state electrolytes", and "anode").

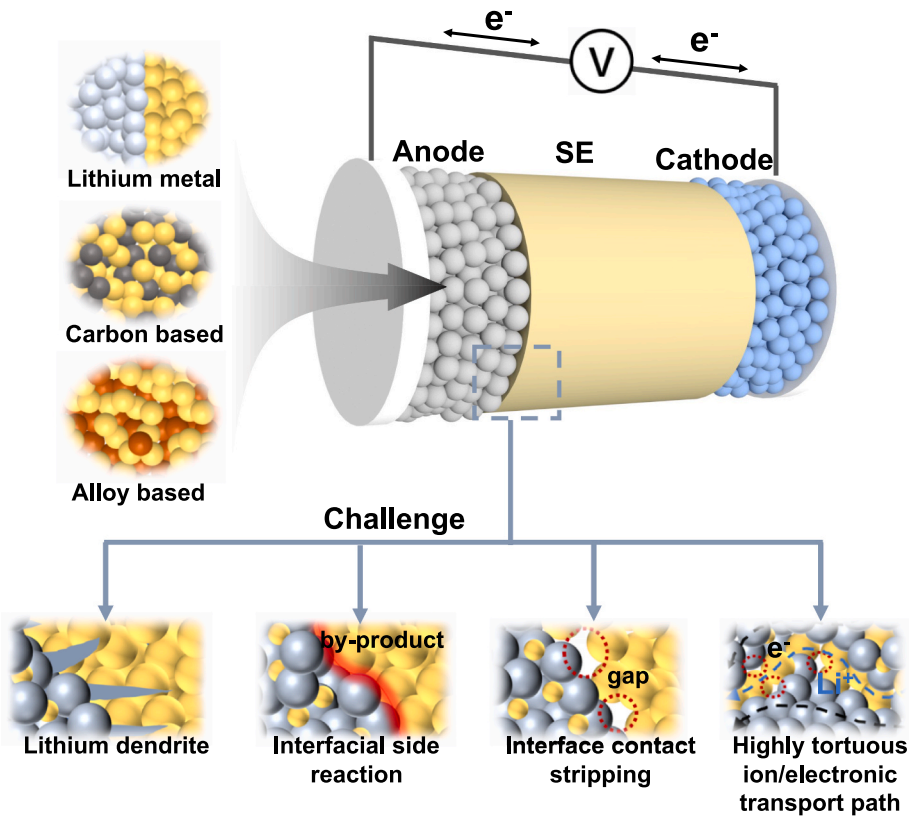

Fig. 2. The components of SSBs and the challenges faced by the anode.

performance. This involves having high electronic and ionic conductivity, as well as a high capacity for storing lithium, while also meeting strict safety regulations and keeping production costs low [32,33]. Therefore, ongoing research and refinement of AAMs are essential to significantly enhance the technological advancement and commercial viability of SSBs [34].

Currently, the focus of research on AAMs for SSBs generally revolves around lithium metal, carbon-based materials, and alloys, each offering distinct advantages due to their unique properties (Table 1). When evaluating battery energy density, lithium metal is an excellent choice for the reasons mentioned above. However, the application of lithium metal anodes in solid-state environments faces several challenges, which are described below. Firstly, during battery operation, the dissolution (stripping)/deposition (plating) of lithium is accompanied by substantial variations in structure. These changes cause cracking and regrowth of the solid electrolyte interphase (SEI) and the formation of "dead" lithium, both contributing to the loss of electrochemically active material and leading to continuous decline in Coulomb efficiency (CE) [41–43]. Secondly, the rigid structure and poor wettability of SEs make it difficult to accommodate the structural variations of the anode during de-/lithiation. This in turn results in the loosening of physical contact at the interface, leading to uneven lithium deposition and the growth of dendrites, which may cause micro-shorts or short circuits within the battery [44,45]. Thirdly, the high reactivity of lithium metal causes severe side reactions at the interfaces, leading to anode corrosion, reduced efficiency, and rapid degradation of interfacial properties, including increased resistance and hindered ion transport. This instability promotes the formation of lithium dendrites, which can damage the anode, puncture the separator layer, and cause internal short circuits, ultimately reducing the battery's energy density and cycle life. To address the issues mentioned above, the most effective approaches are creating a protective layer on the Li|SE interface and designing three-dimensional (3D) frameworks to serve as a host for the lithium ions. These methods enhance the structural stability of the lithium metal anode, prevent interfacial degradation, and inhibit the growth of dendrites [46,47]. Ultimately, these approaches significantly improve the reversibility and cyclability of lithium metal anodes in SSBs. The section on "lithium metal anode" provides a detailed description of the many strategies used to optimize performance, along with the associated working principles [48,49].

Carbon-based materials are widely used in commercial LIBs due to their high stability [50]. In contrast to lithium metal anodes, carbonaceous materials can store lithium ions via intercalation or (near) surface adsorption-type mechanisms, without undergoing major structural/volumetric changes during cycling [51–53]. However, the relatively slow electrochemical reaction process on the surface of carbon-based materials and their low equilibrium potential result in a limited overpotential tolerance, thereby somewhat preventing fast charging. The

Table 1
Comparison of characteristics of representative anode active materials (The volume expansion rate is defined as the percentage change in volume before and after lithium insertion relative to the initial volume) [35–40].

Material	Theoretical specific capacity (mAh g^{-1})	Electrode potential (V vs. Li^+/Li)	Cycle life (number)	Volume expansion (%)	Safety	Market price ($/ton)
Lithium	3860	–	200–1000	~120	poor	50000–70000
Graphite	372	0.1	> 1000	< 10	good	1000–2000
Silicon	3590	0.4	100–500	~300	moderate	8000–10000

complex composition and structural properties of carbonaceous materials (HC and soft carbon featuring large interlayer spacings, abundant pores, and irreversible active sites) often result in low initial Coulomb efficiency (ICE). Furthermore, due to the high mechanical strength and poor wettability of SEs, they struggle to penetrate carbon-based materials as effectively as liquid electrolytes do, leading to poor interfacial contact with SEs and subsequently exacerbating interfacial resistance. To overcome the challenges posed by the inherent limitations of carbonaceous materials, various surface modification techniques have been explored. These modifications aim to mitigate undesirable side reactions with SEs, enhance both electronic and ionic conductivity, and improve surface adsorption and diffusion properties. By addressing these issues, such modifications can significantly enhance the rate performance and reversible capacity of carbon anodes in SSBs. Additionally, these enhancements contribute to better interfacial stability and reduced resistance, which are critical for improving the overall battery performance. Owing to their exceptional stability and high electronic conductivity, carbon-based materials are frequently employed as additives in the preparation of composite electrodes with lithium metal or alloys, further improving the cycling stability of the anode. For instance, Duan et al. developed a Li-C composite using graphite as an additive, which effectively increased the interfacial wettability of lithium metal [54]. More optimization strategies and examples are described in the section on “carbon-based anode active materials”.

Alloy-based AAMs such as silicon (Si), tin (Sn), aluminum (Al), and their composites exhibit higher lithium-storage capacities than traditional graphite [55]. However, such anodes undergo volumetric changes ranging from 50 to 300 % during de-/lithiation, significantly exceeding those of carbon-based materials [56,57]. In SSBs, the expansion of alloy particles or structures leads to the generation of stresses and strains, which can potentially cause local SE failure and a series of issues, like mechanical degradation or delamination at interfaces. Moreover, in contrast to lithium metal anodes, the mechanical properties vary greatly with the composition. Previous experiments on Si and Sn have revealed a significant decrease in yield strength and Young’s modulus from the pristine materials to the lithiated alloys [58,59]. For instance, the yield strength of Si decreases from 2 GPa to 430 MPa upon full lithiation [60]. Furthermore, due to poor contact between alloy-based AAMs and SEs, the internal ion/electron transfer poses a significant challenge. To address the issues faced by alloy-based anodes and achieve improved electrochemical performance, various effective strategies have been proposed, including nanostructuring, structural modifications, and composite formation with other materials. Trevey et al. used multi-walled carbon nanotubes as conductive additive, establishing an efficient electron and ion transport network that doubled the capacity of the Si anode and ensured longevity [61]. Aside from introducing SEs into the electrode to establish ionically conductive pathways, selecting materials with both high ionic and electronic partial conductivities as additives is also a straightforward approach. Dunlap et al. employed heat-treated polyacrylonitrile both as a binder and as a conductive additive for Si anodes, realizing AAM contents of up to 70 % in the electrode and significantly enhancing the energy density [62]. Further elaboration on the optimization strategies for alloy-based anodes will be presented in the section on “alloy-based anode active materials”.

Solid electrolytes

SEs, forming the backbone of SSBs, have been the focus of much attention recently [63,64]. Ideal SEs typically exhibit several crucial properties, including low electronic conductivity ($\sigma_{elec} \leq 10^{-7}$ mS cm^{-1}), high ionic conductivity ($\sigma_{ion} \geq 1$ mS cm^{-1}), excellent chemical compatibility with electrode active materials and other cell components, a wide electrochemical stability window (0–5.0 V vs. Li^+/Li), superior thermal stability, and the ability to be produced on a large scale with significant cost-effectiveness [65,66]. Over the past few decades, researchers have conducted in-depth studies on many different inorganic and polymer SEs, resulting in major improvements in their performance characteristics [67].

Inorganic SEs

Inorganic SEs are classified into several categories, namely oxides, sulfides, halides, nitrides, anti-perovskites, and hydrides. In 2003, Thangadurai et al. [68] made the discovery of garnet-type materials, mainly $Li_5La_3M_2O_{12}$ (M = Ta or Nb, with $\sigma_{ion} \approx 10^{-3}$ mS cm^{-1} at 25 °C). In 2007, Murugan et al. [69] introduced a novel garnet-type SE, $Li_7La_3Zr_2O_{12}$ (LLZO). This electrolyte revealed a high ionic conductivity of 0.1 mS cm^{-1} at 25 °C, along with favorable thermal and chemical stabilities. LLZO derivatives have made significant progress since then. The ionic conductivity of LLZO-type SEs can be enhanced by introducing elements such as Ta, Al, Ga, Nb, W, or Te [70]. For instance, Qin et al. conducted an experiment where they synthesized Ga_2O_3-substituted LLZO (i.e., $Li_{6.55}Ga_{0.15}La_3Zr_2O_{12}$), achieving a high ionic conductivity of 2.06 mS cm^{-1} at 25 °C [71].

Sulfur exhibits a lower electronegativity and a larger ionic radius when compared to oxygen, which results in weaker bonding with lithium and fast ion transport in the respective sulfides [75]. Generally, these SEs possess high ionic conductivities (e.g., Li_6PS_5Cl with $\sigma_{ion} \geq 1$ mS cm^{-1} at 25 °C), approaching or even exceeding that of liquid electrolytes, which can make SSBs also interesting for high-power applications [76]. Sulfide SEs are also notable for their soft mechanical properties, characterized by a low modulus of elasticity [77]. This allows for close particle-to-particle contact, even upon cold pressing, setting them apart from oxide SEs. However, sulfide SEs have a limited electrochemical stability (e.g., Li_6PS_5Cl: 1.7–2.0 V vs. Li^+/Li, see Fig. 3) and poor compatibility with electrode active materials, which may negatively affect battery performance [78]. Furthermore, the commercial use of sulfide SEs is restricted due to the combination of expensive raw materials.

Sulfides are highly sensitive to moisture, readily reacting with water (and oxygen) in the atmosphere, resulting in the formation of toxic H_2S, thus necessitating strict safety measures for their manufacture, transport, and handling [79,80]. Based on the mechanisms of interfacial reactions and lithium dendrite growth, strategies such as constructing artificial (interfacial) buffer layers or doping have been employed to improve sulfide SEs, aiming at effectively suppressing parasitic reactions while achieving superionic conductivity and maintaining low electronic conductivity. Fan et al. prepared a LiF-rich SEI by infiltrating a highly concentrated LiFSI/DME solution into Li_3PS_4, thereby mitigating lithium dendrite growth and adverse side reactions [81].

Halide SEs, in particular those with the formula Li-M−X (where X represents I, Br, Cl, F, and M stands for a metal), have recently garnered attention due to their unique properties, including high oxidation potential ($\geq$ 3.6 V vs. Li^+/Li, see Fig. 3) and moderate ionic conductivity ($\sigma_{ion} \approx$ 1.0 mS cm^{-1}) [82,83]. Despite their improved air stability compared to sulfide electrolytes, halide SEs still face challenges, particularly irreversible hydration reactions in humid environments. These reactions lead to the formation of hydrates such as $MCl_3{\cdot}xH_2O$ and $LiCl{\cdot}xH_2O$, which can further convert into M_2O_3 and corrosive HCl, thus significantly reducing ionic conductivity. To address these issues, anion regulation serves as a critical strategy. Because of the high electronegativity of fluoride ions, their high formation potential (2.87 V vs. Li^+/Li), and small ionic radius, fluorides exhibit the widest electrochemical stability window or, in other words, the best oxidation stability among various halide SEs. Simultaneously, their low hydrophilicity also imparts them with superior air stability. Adjusting the valence state and ionic radius of the central metal species has also been identified as a promising approach to enhance the air and moisture resistance of halide SEs [84]. Based on first-principles calculations, Zhu et al. demonstrated that ternary sodium chlorides containing lanthanide ions (Tm^{3+}, Er^{3+}, Ho^{3+}, Tb^{3+}, etc.) exhibit good moisture stability. Lithium (ternary) chlorides containing trivalent metal ions (In^{3+}, Ga^{3+}) and transition

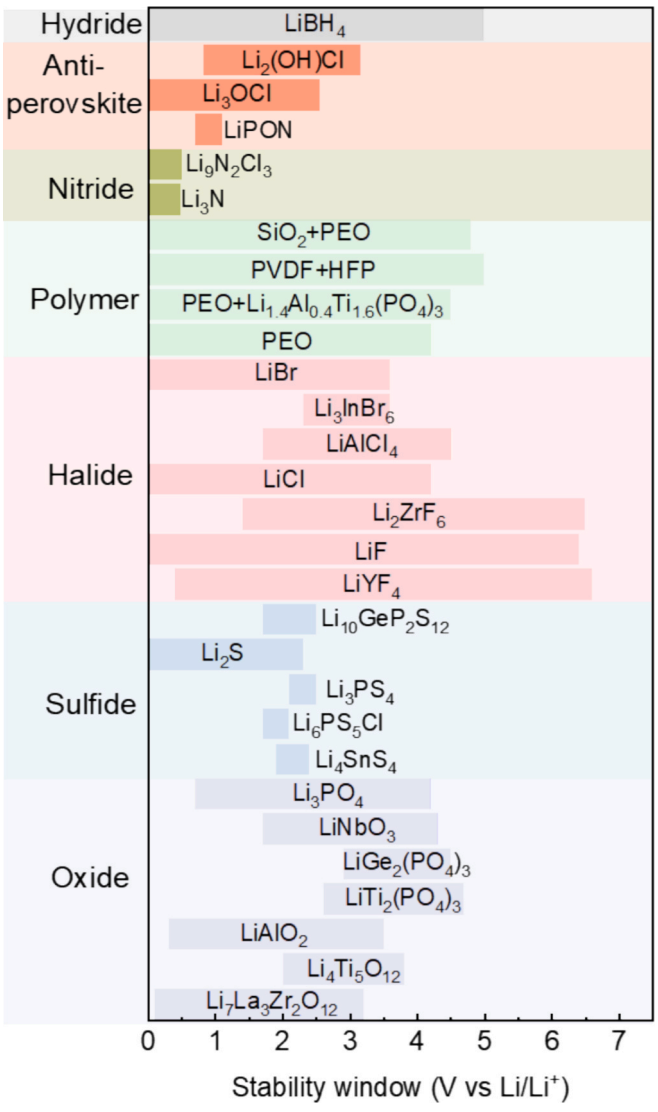

Fig. 3. Comparison of electrochemical stability windows of various types of SEs [72–74].

metal ions (Cd^{2+}, Zn^{2+}) also possess favorable moisture stability, with Li_3InCl_6 exhibiting high resistance, consistent with experimental reports of its exceptional humidity tolerance [84]. Furthermore, structural tailoring and surface coating have been validated as reliable methods for improving the air stability of halide SEs. Li et al. found that $Li_3Y_{1-x}In_xCl_6$ ($x > 0.5$) can maintain a room-temperature ionic conductivity of up to 1.05 mS cm^{-1} even after exposure to 3–5% humid air, which is primarily attributed to the preferential formation of the hydrated, intermediate phase, $Li_3(Y_{1-x}In_x)Cl_{6-x}H_2O$ [85]. Additionally, Wang et al. successfully enhanced the moisture resistance of Li_3InCl_6 by applying an Al_2O_3 protective surface layer via atomic layer deposition, which only led to a slight decrease in ionic conductivity [86].

In addition to conventional SEs, emerging materials such as nitrides, anti-perovskites, and hydrides exhibit low densities and good interfacial stabilities. Nitride SEs, including lithium nitrides (e.g., α/β-Li_3N), LiPON, lithium nitrogen halides (e.g., $Li_9N_2Cl_3$), and lithium nitrogen sulfides, may possess reasonably high ionic conductivities (e.g., β-Li_3N with σ_{ion} = 0.21 mS cm^{-1} at room temperature) enabled by defect engineering [87]. For instance, in α-Li_3N with a hexagonal lattice, Li^+ rapidly diffuses via vacancies between Li_2N layers, while β-Li_3N relies on vacancies at the Li(4f) sites to reduce diffusion barriers [88,89]. $Li_9N_2Cl_3$ further enhances the room-temperature conductivity (0.043 mS cm^{-1}) through synergistic effects of high-concentration Li, N, and Cl vacancies [90]. These materials form stable decomposition phases (e.g., Li_3N/Li_3P) upon contact with lithium metal, effectively suppressing side reactions and reducing interfacial impedance, thereby improving cycling stability and safety. Notably, their synthesis methods (e.g., ball milling and thermal treatment) align closely with sulfide/halide SE protocols, enabling cross-system optimization strategies.

Anti-perovskite SEs (e.g., Li_3OCl), with their tailorable ion transport channels and good interfacial stability with lithium metal, are becoming attractive for use in SSBs. However, they still face intrinsic limitations. Most reported anti-perovskite SEs exhibit extreme moisture sensitivity, readily decomposing into proton-rich compounds or hydrates that may introduce unfavorable protonic and/or electronic conduction. The decomposition phases between anti-perovskite SEs and lithium metal remain poorly characterized, significantly limiting understanding of stabilization mechanisms at the anode interface. Furthermore, anti-perovskite SEs typically possess high hardness but low ductility, making them prone to loss of ionic and electronic conduction pathways following electrode volume changes during cycling. Addressing these challenges requires (i) fundamental investigations into conduction mechanisms within anti-perovskite SEs, (ii) detailed characterization of SE|anode interfaces, and (iii) systematic studies on their structural integrity during cycling [74].

Hydride electrolytes, exemplified by $LiBH_4$, demonstrate high ionic conductivity (>1.0 mS cm^{-1}) in the high-temperature phase (HT-$LiBH_4$, > 120 °C) but suffer from poor conductivity (~10^{-3} mS cm^{-1}) in the low-temperature phase (LT-$LiBH_4$) [91]. While their low density (0.67 g cm^{-3}) offers potential for the development of high-energy–density batteries, critical drawbacks persist: (i) limited oxidation stability (< 2.8 V vs. Li^+/Li) caused by the presence of H^- anions hinders compatibility with high-voltage cathodes, (ii) difficulties in modifying complex anionic species (e.g., BH_4^-) restrict conventional doping strategies, and (iii) temperature-dependent conduction mechanisms limit practical applicability. Recent studies have shown that mechanochemical compositing with oxides helps improve electrochemical stability, though interfacial dynamics remain unresolved [92]. Collectively, while sulfide/halide systems clearly outperform these rather "exotic" SEs, their distinct structural features and transport mechanisms open new dimensions for fundamental research and technological innovation in SSBs.

Polymer SEs

In contrast to inorganic SEs, polymer SEs offer notable advantages such as high flexibility, good interfacial contact, and superior processability. Particularly, the high adhesion of polymer SEs helps accommodate the volume changes of electrodes during charge and discharge. This attribute not only improves the stability of the electrode|electrolyte interface but also reduces the resistance associated with interfacial charge transfer [93–95].

Polymer-type SEs are composed of a polymer matrix such as polyethers, polysiloxanes, or polycarbonates combined with alkali metal salts [96,97]. Polyether SEs feature electron-donating ether oxygen (–C–O–C–) functionalities, which enhance their compatibility with lithium metal in terms of electrochemical properties [98]. Prominent polymers in this category include polyethylene oxide (PEO) and poly (ethylene glycol) methacrylate (PEGMA). PEO is notable for its ease of film formation, good compatibility with lithium metal, and high chemical stability, making it a widely studied polymer SE [99]. On the other hand, PEGMA exhibits a gel-like consistency and shows favorable ionic conductivity (0.01 mS cm^{-1}) at room temperature. Although PEGMA's ability to form films is limited and lacks mechanical strength, it is beneficial in producing polymer SEs through *in situ* solidification within porous membranes [100].

Polysiloxane SEs are characterized by high thermal stability, low toxicity, and environmental friendliness. However, their practical

applications are restricted by poor mechanical strength, attributed to a low glass transition temperature (from −60 to −120 ℃) [101]. To enhance the mechanical strength of polysiloxane SEs, certain functional groups can be introduced using chemical modification methods such as grafting, cross-linking, or copolymerization, taking advantage of the reactivity of Si–H and C═C bonds [102]. Walkowiak et al. synthesized a novel lithium-ion carrier polymer through a hydrosilylation reaction using the hydrogen atoms of polysiloxane and the double bonds of vinyltris(2-methoxyethoxy)silane as "catalysts". Employing $LiPF_6$ as lithium salt, this electrolyte forms efficient ion transport pathways along the backbone of the polymer chain. When the molar ratio of polymer-to-lithium salt reaches 40:1, its ionic conductivity at room temperature can reach 1.12 mS cm^{-1} [103].

Polycarbonate SEs, including polypropylene carbonate and polyethylene carbonate, feature carbonyl groups that bind with lithium ions. Compared to the ethylene oxide groups in PEO, the coordination of carbonyl and carbonate groups with lithium ions is weaker, resulting in higher mobility [104]. The uniqueness of polycarbonates lies in their amorphous nature and flexible segments, containing polar carbonate groups and, thus, possessing high dielectric constant. This structure endows polycarbonate-based SEs with significant advantages in terms of electrochemical and thermal stabilities. Chai et al. successfully obtained a poly(vinylene carbonate)-based SE with good performance through *in situ* polymerization of vinylene carbonate (VC) induced by lithium difluoro(oxalate)borate (LiDFOB). Goodenough et al. reported a cross-linked polyethylene glycol methyl ether acrylate (CPMEA) as electrolyte, wherein the polyacrylate provides a stable 3D framework, while the low-polymerized ethylene oxide attached to the framework can move freely, thereby facilitating lithium transfer. This SE achieves an ionic conductivity of 0.1 mS cm^{-1} at 60 °C [105].

Overall, polymeric SEs can establish improved physical contact with the AAMs and enhance the chemo-mechanical stability at the AAM|SE interface due to their superior flexibility and ease of processing. However, the utilization of polymer SEs is constrained by inherent issues such as poor lithium ion transference number ($t_{Li+} \approx 0.2$–0.3), relatively low conductivity, insufficient electrochemical stability, and limited mechanical stability [low shear modulus (1–10 GPa)]. Note that these problems can be resolved by transitioning from polymeric to inorganic SE. These two types of electrolytes have complementary properties. Therefore, based on the characteristics of the electrode active materials, it is of paramount importance to carefully select or design suitable (composite) SEs to construct stable interfaces for high-performance SSBs. Figs. 3 and 4 provide an overview of the properties of various SEs.

Effect of various SEs on anode

The performance of SSB anodes is greatly influenced by the inherent characteristics of the SE and its compatibility with the AAM [106,107]. First, these two factors are strongly correlated with the occurrence of electrochemical and/or chemical side reactions at the interface [108]. To be specific, sulfide and halide SEs are particularly prone to undergoing decomposition because of their unfavorable reduction potentials (e.g., Li_6PS_5Cl yields Li_2S, Li_3P, and LiCl, thus increasing interfacial resistance), although the composition of byproducts varies significantly. During this process, the sulfides generate interfacial byproducts that have the property of being electronically insulating [109]. This means, they are capable of forming a "stable" SEI, which effectively prevents additional interfacial reactions [110]. In contrast, decomposition products from halide SEs may exhibit some electronic conductivity, potentially exacerbating side reactions and degrading battery performance (e.g., Li_3InCl_6 undergoes electrochemical reduction at low potentials, generating indium metal and LiCl) [111]. It is worth noting that oxide SEs such as LLZO, with an electrochemical stability window of about 0.05–3.2 V vs. Li^+/Li (see Fig. 3), usually exhibit better chemical and electrochemical stability, which reduces the likelihood of reductive decomposition at the interface [112,113]. Unfortunately, they are prone to reaction with humid air leading to the formation of LiOH and Li_2CO_3, which degrade the interfacial compatibility woith AAMs.

Furthermore, unlike liquid counterparts, SEs are usually unable to infiltrate the AAM (of note, the same holds for proper surface wetting) due to their intrinsic mechanical rigidity. This typically results in a point-to-point particle contact mode between SEs and AAMs, limiting charge-carrier transport across the interface. Importantly, during battery operation, structural (volume) changes of the AAM induce loss of physical contact with the SE, leading to electro-chemo-mechanical degradation. This in turn results in the formation of electrochemically

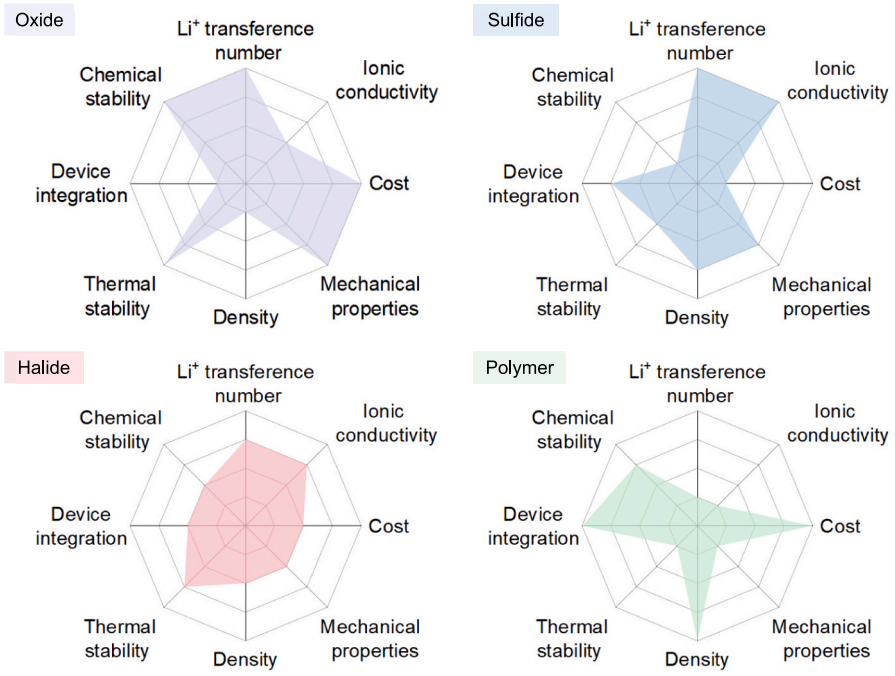

Fig. 4. Comparison of the main characteristics of state-of-the-art SEs [83].

inactive (spatial) regions at the interface and significant impedance buildup. In this regard, oxide SEs having the greatest hardness face major difficulties in accommodating volume changes of AAMs upon repeated de-/lithiation [33]. Conversely, sulfide and polymer SEs possess more favorable characteristics (having a low Young's modulus), which can somewhat mitigate this issue and enable improved physical interaction with AAMs [114]. Based on the above discussion, it is clear that ensuring robust physical contact between the SE and the AAM is essential for maintaining fast (interfacial) transport in SSBs. Large-scale application of halide SEs is limited by their intrinsic cathodic instability. This challenge can be addressed through synergistic optimization strategies combining lattice engineering, interface passivation, and composite design to enhance interfacial stability and cyclability. However, this increases battery cost and reduces energy density, hence diminishing the potential of halide SEs for extensive implementation [115]. Therefore, in developing advanced anodes for SSBs, it is essential to thoroughly analyze the properties of SEs and AAMs across various aspects, including ionic conductivity, ion-storage capacity, electro-/chemical stability, material density, cost, and mechanical properties.

Overall, high-performance (composite) anodes can be constructed by matching suitable AAMs with specific SEs, combined with material optimization techniques such as coating, doping, surface modification, and compositing. In the following chapters, we will sequentially introduce the design of promising anode structures and components based on lithium metal, carbon, and alloy-type AAMs.

Lithium metal anode

The intrinsic properties of lithium metal make it attractive for application as a next-generation anode [73,116–118]. However, its practical implementation in SSBs faces multiple challenges. Firstly, superionic SEs, with their higher mechanical rigidity compared to liquid counterparts, can partially inhibit the growth of dendrites. However, the grain boundaries provide pathways for dendrite propagation, emerging as a key factor responsible for short circuiting and SSB failure. Secondly, the chemical incompatibility between lithium metal and the majority of inorganic SEs leads to continuous formation of interfacial byproducts, negatively affecting ion transport. Furthermore, the volume changes induced by lithium deposition/stripping during cycling create mechanical stress mismatches with the rigid structure of SEs, resulting in interfacial contact failure [119,120]. These coupled effects pose fundamental challenges to the long-term stability and safety of lithium metal anodes, constituting critical bottlenecks that must be overcome for the industrialization of SSBs. Nevertheless, leveraging the rigidity of SEs to inhibit dendrite growth is expected to enable widespread application of lithium metal anodes in SSBs, which will significantly boost the energy density [121].

Recent studies revealed that the nucleation and growth of lithium dendrites still exist in the solid-state environment, occurring not only at the anode side but also forming between SE grains, albeit not as severe as in the liquid counterpart [122,123]. This potentially causes micro-short circuiting or even complete short circuiting [124,125]. The dendrite problem in SSBs is primarily caused by the point-to-point contact mode of electrochemically active materials [126,127]. This type of contact leads to an uneven distribution of charge carriers at the interface, resulting in excessive localized ion concentration and the nucleation and growth of lithium dendrites [128,129]. Of note, this problem becomes more serious due to the large volume changes of the lithium metal anode during battery operation and the poor wettability of the SE [130]. While applying external pressure in SSBs can ensure adequate contact between the lithium metal and the SE, excessive pressure may induce lithium deformation and penetration into the electrolyte, ultimately degrading battery performance. Zhao et al. proposed a strategy to address this challenge by incorporating 3 at.% magnesium (Mg) into lithium, thereby altering its strain-hardening behavior [131]. The Li-Mg alloy anode demonstrates the ability to withstand high fabrication pressures (50–65 MPa) without electrolyte penetration. Symmetrical cells with Li-Mg electrodes exhibited a critical current density 200 % higher than that of lithium metal electrodes. Furthermore, LePage et al. elucidated the general relationship between strain rate and current density, revealing that power-law creep dominates as the primary deformation mechanism across a wide range of battery-relevant conditions [132]. This work bridges the battery and mechanics communities in an innovative manner, providing a foundational framework for understanding coupled electro-chemo-mechanical phenomena in lithium-based systems [133]. Additionally, due to the highly reactive nature of lithium metal, severe interfacial side reactions occur between the SE and the anode during cycling. These reactions not only lead to the loss of electrochemically active material and the emergence of dendrites but also result in a sharp increase in interfacial impedance, ultimately causing rapid battery degradation. For instance, Li_6PS_5Cl has attracted significant attention due to its room-temperature ionic conductivity exceeding 1 mS cm^{-1} and excellent processability. However, it suffers from a narrow electrochemical stability window and forms an unfavorable SEI on the lithium metal anode (high interfacial resistance). Notably, Leonie et al. proposed an innovative organic additive approach by incorporating prelithiated trithiocyanuric acid into Li_6PS_5Cl. This modification effectively mitigates electrolyte decomposition, eventually leading to a more stable anode interface [134]. Furthermore, the "hostless" nature of lithium metal anodes allows quasi "unlimited" volume changes, leading to poor contact with SEs, high interfacial impedance, and significant voltage hysteresis during operation [135]. These factors collectively promote lithium dendrite growth and simultaneously contribute to the formation of numerous electrochemically inactive regions and dead zones, thus resulting in rapid capacity fade in SSBs. *In situ* scanning electron microscopy (SEM) studies have shown that volume changes can create gaps between Li_3PS_4 and Li_6PS_5Cl SEs and lithium metal, increasing resistance and creating "hotspots" for dendrite growth [136]. Likewise, discontinuous contact between lithium metal and SEs results in lithium deposition solely at the contact points, which then also become "hotspots" for dendrite growth. In addition, the random distribution of side products within the mixed conducting layer leads to varying ionic conductivities, further exacerbating the uneven concentration of Li^+ at the anode surface and accelerating dendrite growth. The combination of these factors often results in poor cyclability of lithium metal anodes, being a core challenge to be addressed in the SSB field (Fig. 5).

Protective coatings

Applying a protective coating to the surface of lithium metal serves

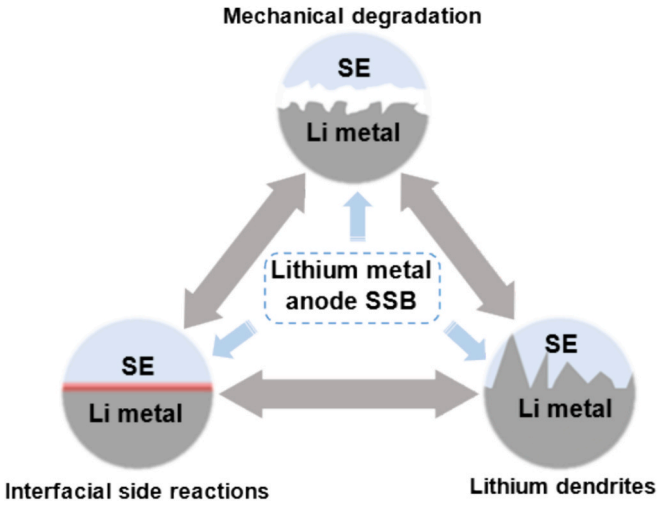

Fig. 5. Challenges faced by the lithium metal anode in SSBs.

as an efficient and straightforward approach to tackle the challenges faced by such anodes in SSBs [137–139]. The purpose of this is to form a robust layer on the surface, isolating it from physical (electronic but not ionic) contact with the SE, thereby inhibiting unwanted electro-/chemical reactions [140–142]. In general, the protective layer should allow for fast ion transport to ensure uniform lithium flux and prevent dendrite initiation. Simultaneously, it must demonstrate mechanical strength and flexibility, enabling stress endurance during dendrite propagation while accommodating the dynamic volume changes of lithium metal during cycling. Furthermore, an ideal protective layer requires chemically inert interfaces with both lithium metal and SE to avoid generating unstable interphases through parasitic side reactions

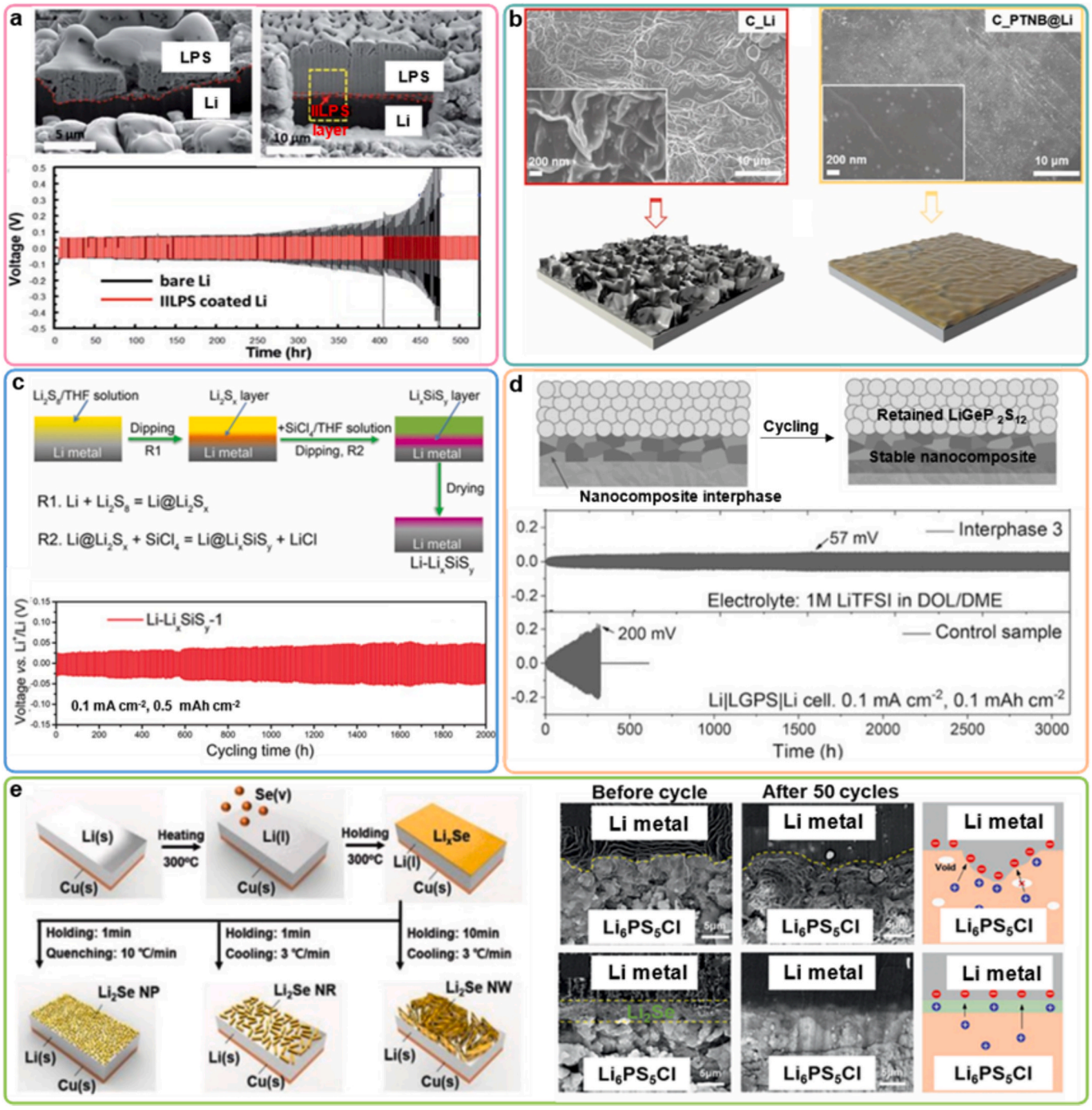

Fig. 6. Protective coatings for lithium metal anodes. (a) SEM images of the IILPS layer between Li metal and LPS SE and galvanostatic testing of symmetric cells with lithium and IILPS-coated lithium anodes at a current density of 0.5 mA cm^{-2}. Reproduced from ref. [146]. Copyright 2022, with permission from The Royal Society of Chemistry. (b) *Ex situ* morphology investigations of recovered C-Li and C-PTNB@Li electrodes. Reproduced from ref. [148]. Copyright 2021, with permission from Wiley-VCH. (c) Schematic illustration of the *in situ* formation process of Li-Li_xSiS_y and its long-term cycling performance. Reproduced from ref. [149]. Copyright 2019, with permission from Wiley-VCH. (d) Illustration of lithium salt-based organic–inorganic nanocomposite as protective layer for stabilizing the Li|$Li_{10}GeP_2S_{12}$ interface, along with the voltage profiles of Li deposition in Li|$Li_{10}GeP_2S_{12}$|Li cells. Reproduced from ref. [150]. Copyright 2018, with permission from Wiley-VCH. (e) Illustration of synthesis procedures for nanostructured Li_2Se on lithium metal by CVD, cross-sectional SEM images of lithium metal and Li/Li_2Se cells before and after 50 cycles at 0.1 mA cm^{-2}, and scheme of the charge distribution at the interface. Reproduced from ref. [151]. Copyright 2021, with permission from Wiley-VCH.

(interfacial impedance buildup) [143–145].

Lee et al. employed a solution method to synthesize an interlayer (IILPS) comprising a Li_2S-P_2S_5 (LPS) glass–ceramic matrix, an In/InLi alloy, and LiI (Fig. 6a) [146]. This interlayer serves to stabilize the lithium metal anode by protecting it from interfacial instability. The resulting seamless interface between lithium and LPS, coupled with the chemical compatibility of the interlayer with the SE, allows for intimate contact within the anode structure. The lithium transport facilitated by the IILPS ensures even deposition of lithium beneath the interlayer. The key to advancing the development of lithium metal in SSBs lies in achieving stable performance through simple processing methods. Wang et al. utilized lithium foil as anode and treated it with an organic solution containing SbF_3 using a spraying technique, thereby generating an artificial LiF/Li_3Sb SEI. The study revealed that lithium preferentially deposits in the gaps between the LiF/Li_3Sb particles, gradually covering the interfacial layer and forming a uniform (dense) layer on the surface. This process effectively enhances the stability of the lithium|SE interface and mitigates dendrite formation and the risk of short-circuiting [147]. Passerini and colleagues coated lithium metal with a thin layer of poly [2,3-bis(2,2,6,6-tetramethylpiperidine-N-oxycarbonyl)norbornene] (PTNB) using a simple dip-coating method, together with a high concentration of lithium in an ionic liquid electrolyte (0.4LiFSI-0.6Pyr_{14}FSI), to prevent direct contact between $Li_{1+x}Al_xTi_{2-x}(PO_4)_3$ and lithium [148]. PTNB aids in the uniform distribution of lithium ions, thus impeding the formation of dendrites (Fig. 6b). Without the PTNB coating, the lithium stripping/plating lifespan concludes after 128 h. However, using PTNB@Li, it can be extended to ~800 h of dendrite-free operation. Nevertheless, unlike the dip-coating method, *in situ* formed coatings provide more uniform and complete coverage, further enhancing the lifetime of SSBs. For instance, Liang et al. demonstrated that the Li_xSiS_y layer formed *in situ* on the surface of lithium metal stabilizes the Li|Li_3PS_4 interface (Fig. 6c) [149]. Remarkably, this layer also shows high stability in air. The components of the Li_xSiS_y layer, i.e., Li_2SiS_3 and Li_4SiS_4, facilitate ion transport, while the Li_2S in direct contact with the lithium prevents interfacial side reactions. Tests revealed that symmetric cells with Li_xSiS_y-coated lithium anodes maintain stable performance for over 2000 h. Gao et al. utilized a nanocomposite comprising organic elastomer salts (LiO–$(CH_2O)_n$–Li) and inorganic nanoparticle salts (LiF, –NSO_2–Li, Li_2O) [150]. They achieved lithium deposition for more than 3000 h and demonstrated a good cycle life of Li|$Li_{10}GeP_2S_{12}$|TiS_2 cells, while bare samples showed less than 500 h of stable lithium deposition (Fig. 6d).

At the same time, regulating the structure of the coating is also crucial to improving the performance of SSBs. Park et al. successfully grew nanostructured Li_2Se (epitaxially) as a protective layer onto the surface of lithium metal by chemical vapor deposition (CVD) [151]. By controlling the reaction time and cooling rate, the morphology of Li_2Se could be manipulated to produce nanoparticles, nanorods, or nanowalls with different orientations, aligning the (220) plane parallel to the (110) plane of the lithium substrate (Fig. 6e). This process established robust chemical bonds between the Li_2Se layer and the lithium metal, ensuring a proper physical interface with the Li_6PS_5Cl SE. This demonstrates that the two materials are compatible with the as-constructed Li_2Se, which helps effectively mitigate undesired side reactions and further facilitates uniform charge transfer across the interface during cycling, eventually leading to significant improvements in battery performance and stability.

Structural engineering

Designing advanced micro-/nanostructures for lithium metal can reduce the local current density and provide abundant nucleation sites, both of which helps suppress the growth of lithium dendrites [152]. This kind of strategy can lead to enhanced cycling stability, safety, and performance of the lithium metal anode, providing strong support for the development of high-performance SSBs [153].

Constructing 3D anodes has proven to be the most effective strategy for addressing the dendrite issue in liquid electrolyte based batteries. However, the rigid nature of inorganic SEs limits solid–solid ionic contact at the interface. Duan et al. utilized a spontaneous chemical reaction between halides and lithium metal to *in situ* form a 3D anode. The formed alloy acts as a lithiophilic matrix, reducing the nucleation overpotential of lithium and promoting uniform nucleation and deposition [154]. Han and colleagues employed a hot-pressing method to fabricate a lithium metal anode containing a 3D carbon skeleton/copper collector (CP/Cu) [155]. The LiC_x layer that naturally forms on the surface of the CP skeleton provides numerous sites and reduces the overpotential for lithium nucleation, thereby promoting dense deposition (Fig. 7a). Moreover, the high surface area of the conductive CP skeleton helps lower the local current density and therefore the likelihood of dendrite growth, thus restraining volume fluctuations in the anode.

Efforts to prevent the formation of lithium dendrites using simple techniques have consistently been a goal. Yang et al. devised a method to deposit lithium in a targeted manner [156]. They divided the anode into numerous square pieces with deep grooves (Fig. 7b). The high current density within these grooves causes lithium to selectively deposit in them rather than on the surface, thereby preventing the formation of dendrites during the plating/stripping process. Metal-organic frameworks (MOFs) have garnered significant attention in the field of energy storage due to their design flexibility, distinct physicochemical characteristics, and broad range of potential use [157]. Wang et al. proposed employing a carbonized MOF (Co-MOF) nanorod array modified carbon cloth (NRA-CC) as support structure [158]. The Co-MOF generates cobalt and nitrogen atoms during the carbonization process, which effectively converts the lithiophobicity of carbon materials into lithiophilicity, enhancing the deposition process. Concurrently, dendrite growth is effectively suppressed by minimizing the local current density and restricting volume variations within the 3D porous network structure. In addition, they also devised a 3D anode produced using a melt-infusion strategy. In conventional 2D lithium foil, the Li^+ flux concentrates at the protuberance tips, leading to the appearance of dendrites and inactive lithium. Conversely, when it comes to 3D anodes, lithium tends to form and spread onto the surface of the 3D framework. This promotes uniform distribution of ions throughout the structure, which in turn helps prevent the formation of dendrites [159].

Composites

Functional inorganic materials provide multidimensional solutions for performance optimization in mitigating the growth of lithium dendrites through their unique physicochemical properties. Serving as additives, these materials establish three-dimensional conductive networks in lithium metal composite anodes to enhance charge transfer while inducing uniform lithium deposition via chemical modulation of surface functional groups, effectively mitigating local electric field distortions. Furthermore, their interfacial modification capabilities dynamically regulate the electrode surface chemistry, forming ionically conductive and mechanically stable (adaptive) interfacial layers during cycling [108]. Chen et al. designed a composite anode for SSBs by combining molten lithium with 1D TiO_2 nanofibers [160]. The surface tension of the lithium metal was significantly reduced, greatly improving interfacial contact with the $Li_{6.5}La_3Zr_{1.5}Ta_{0.5}O_{12}$ SE and facilitating lithium plating and stripping. g-C_3N_4 possesses a layered structure similar to graphite with abundant amino and Lewis basic groups, as well as a high nitrogen content, which contributes to achieving efficient charge transfer. Hang et al. incorporated g-C_3N_4 into lithium metal, resulting in a substantial increase in viscosity at the interface [52]. This enhancement effectively prevented dendrite formation. Li-C_3N_4|garnet SE|Li-C_3N_4 cells exhibited good performance, with an extremely low interfacial resistance of 11 Ω cm^2 and a high critical current density of 1500 μA cm^{-2}. In contrast, the same cell

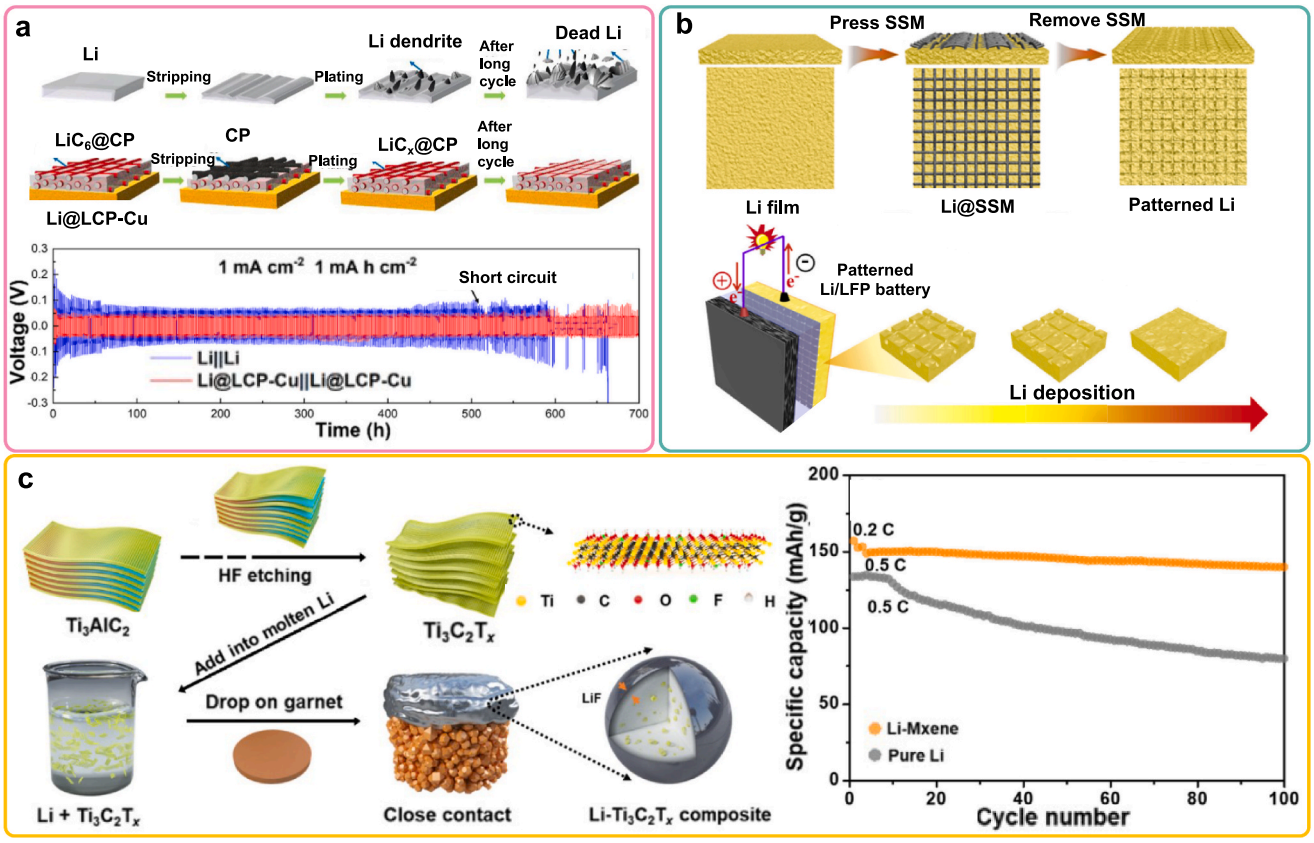

Fig. 7. Structural and compositional engineering of lithium metal anodes. (a) Schematic representation of the mechanism for the improved performance of Li@LCP-Cu anodes, and the voltage profiles of symmetric cells with commercial Li and Li@LCP-Cu electrodes. Reproduced from ref. [155]. Copyright 2023, with permission from Elsevier. (b) Schematic illustration of patterned Li fabrication, and the Li deposition process. Reproduced from ref. [156]. Copyright 2020, with permission from Elsevier. (c) Synthesis process of MXene, Li-MXene composite, and the interfacial contact of Li-MXene|garnet, along with the cycling performance comparison of Li-MXene|garnet|$LiFePO_4$ and Li|garnet|$LiFePO_4$ cells. Reproduced from ref. [161]. Copyright 2022, with permission from Elsevier.

configuration using the original lithium metal revealed a much larger interfacial resistance of 428 Ω cm^2 and a lower critical current density of 50 μA cm^{-2}. Wen et al. used MXene as an additive to prepare Li-MXene composites [161]. The interaction between molten lithium and the fluorinated functional groups present on the MXene resulted in the formation of an insulating LiF layer at the Li-MXene|garnet interface, which inhibits the formation of dendritic lithium. In addition, the presence of rich surface functional groups (–OH or –F) provides the Li-MXene composite anode with a very high capacity (Fig. 7c).

Anode-less design

Anode-less designs eliminate the use of AAMs, maximizing the energy density at the cell level [162–164]. Ideally, during the initial charge, lithium ions are released from the cathode and evenly deposited on the counter electrode. In the subsequent discharge, the ions return to the cathode host, achieving 100 % utilization of lithium and resulting in substantial cost reduction [165]. However, without a stable host material at the anode side, irreversible losses due to the formation of "dead" lithium and/or side reactions with the SE during cycling directly cause the battery capacity to fade [30]. Moreover, during lithium deposition and stripping, the volume variations of the anode can lead to significant internal stress changes, potentially damaging the structure of the SE [166]. To improve the reversibility of anode-less SSBs, it is necessary to inhibit detrimental electro-/chemical reactions and facilitate the formation of a favorable deposition structure on the current collector (CC). This will ensure a well-formed (conformal) interface with the SE. Current strategies to enhance cyclability mainly focus on SE and interface design, as well as on CC modification [121,167,168].

Constructing functionalized CCs that enable uniform and stable deposition and extraction of lithium ions is an effective modification strategy for anode-less SSBs. Wen et al. coated a layer of Ag nanoparticles onto Cu foil, followed by further covering with a lithiated polyacrylic acid polymer, thereby achieving intimate interfacial contact between SE and Cu [169]. Despite some progress made, the issue of volume expansion remains a significant challenge. Kim et al. employed titanium nitride nanotubes (NTs) and a silver-carbon interlayer to alleviate the stress induced by the repeated formation of lithium deposition layers on Cu foils during cycling [170]. The mixed conducting nature of the titanium nitride NTs helps accommodate the diffusion creep of reduced lithium into the free volume, enabling quasi strain-free operation and offering nearly a tenfold improvement in controlling volume expansion compared to conventional Cu anodes during lithiation. Moreover, the Ag-C interlayer guides the lithium deposition, maintaining a uniform thickness and playing a pivotal role in dendrite suppression and volume stability (Fig. 8a). While notable advances have been made, challenges related to low CE and extensive dendrite growth remain unresolved. Lee et al. employed an Ag-C nanocomposite layer as anode, where the solubility of Ag in Li reduces the nucleation energy, ultimately facilitating uniform deposition on the CC [40]. Simultaneously, the carbon serves as a separator, isolating the SE from the lithium metal. By utilizing a layered Ni-rich oxide cathode and a silver-germanium sulfide SE, SSBs with an energy density exceeding 900 Wh L^{-1} and with a long cycle life (1000 cycles) could be realized (Fig. 8b).

Although these studies indicate improvements in battery performance, the understanding of how interfacial layers affect the evolution

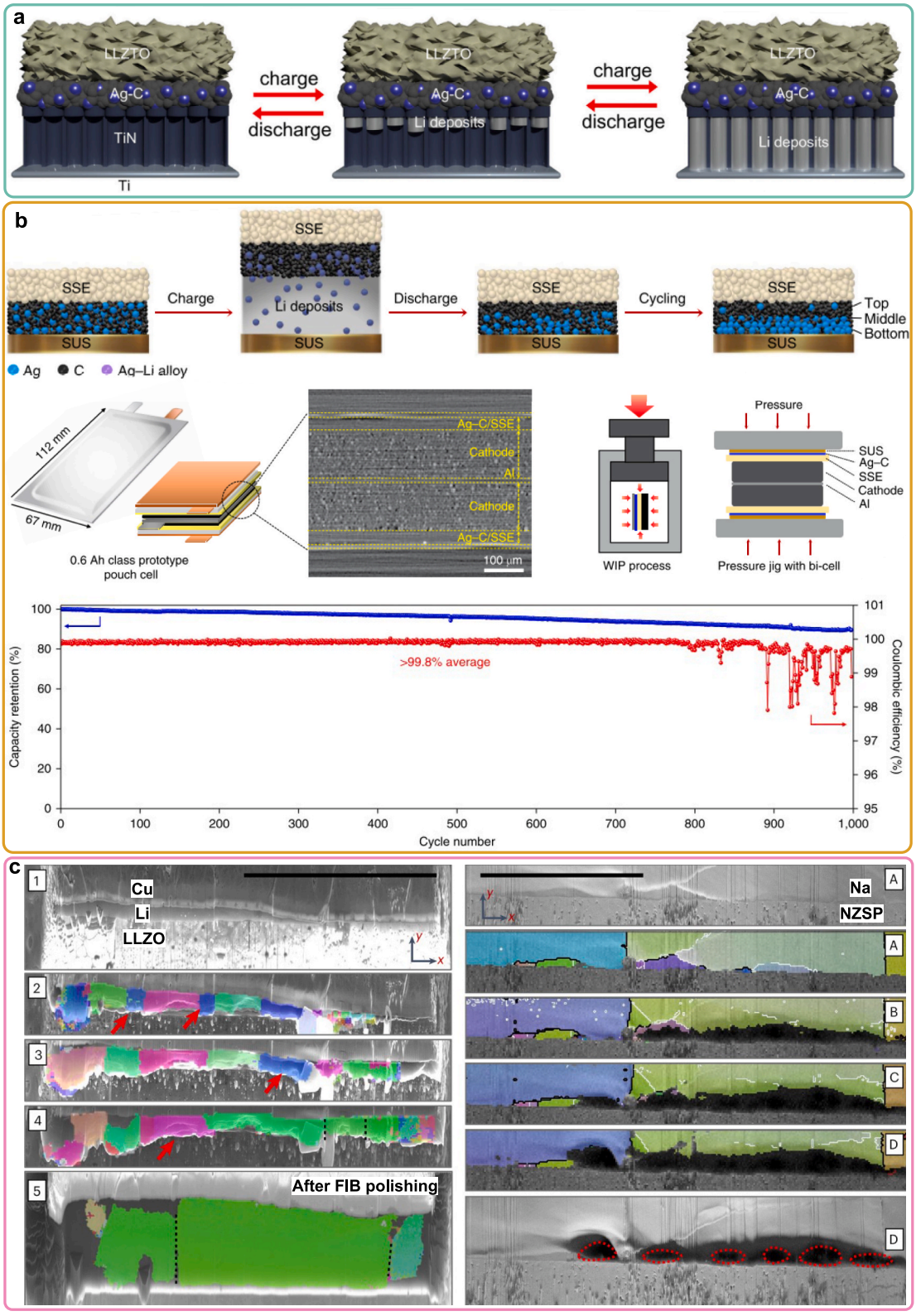

Fig. 8. Anode-less design strategies. (a) Schematic of the TiN NT-incorporated anode-less SSB concept during the charging/discharging process. Reproduced from ref. [170]. Copyright 2024, with permission from Springer Nature. (b) Schematic of lithium plating/stripping onto/from the CC with an Ag-C nanocomposite layer, characterization of prototype pouch cells, illustration of the bilayer cell structure, and cycling performance and CE of an Ag-C|Li_6PS_5Cl|$LiNi_{0.90}Co_{0.05}Mn_{0.05}O_2$ pouch cell plotted against the cycle number. Reproduced from ref. [40]. Copyright 2020, with permission from Springer Nature. (c) Microstructure evolution for lithium plating and sodium stripping. The red arrows indicate grains disappearing during film growth, and the red outlines indicate pores formed during stripping. The map provided in Step 5 was acquired after a 2-week storage period and a second FIB polishing step. Scale bars, 100 μm. Reproduced from ref. [174]. Copyright 2024, with permission from Springer Nature.

of anode-less SSBs remains insufficient. Sandoval et al. investigated the structure and electrochemical evolution of silver and gold alloy interlayers in sulfide (Li_6PS_5Cl) SSBs "without" anode [171]. They found that these materials enable uniform lithium deposition/stripping and mitigate contact loss at the end of stripping through responsive current homogenization. Compared to bare Cu, both alloy layers significantly enhanced the cycling stability and CE. Jun et al. systematically studied and explained the behavior of lithium alloying in anode-free SSBs, based on the different alloying kinetics and the diffusion rates of lithium in the alloy phase [172]. They demonstrated the critical importance of the thermodynamic and kinetic properties of lithium alloy formation in controlling lithium deposition behavior in SSBs. Lee et al. evaluated various metal fluorides and found that the lithium plating kinetics and behavior are largely influenced by the Li-M reaction mechanism [173]. Through comparative analysis of various metal fluorides, AgF was identified as the most suitable (conversion reaction) choice. Various strategies have been reported to control the uniformity (morphology) and density of electrodeposited alkali metal films. However, their microstructure remains unclear, and suitable characterization methods have yet to be established. Fuchs et al. used focused ion beam (FIB) milling and polishing techniques under inert gas or high vacuum and low-temperature conditions, along with a high-sensitivity electron backscatter diffraction system, to reveal the electrochemical growth of large metal grains for the first time (Fig. 8c) [174]. This opens up new avenues for subsequent research on the relationship between the electrochemical performance of alkali metal anodes and their microstructure. Furthermore, the reversibility is compromised by the inability of conventional Al foil to meet the requirement of intimate interfacial contact. To improve upon the contact between SE and CC, Deysher et al. pressed granular Al onto the SE during cell manufacturing, resulting in an Al particle-decorated CC [175]. Unlike pristine Al foil, the granular CC generates a more uniform and intimate interface with the SE, which helps significantly increase the critical current density.

Conclusion

Despite lithium metal anodes being considered ideal candidates due to their high theoretical specific capacity, the uncontrolled growth of dendrites remains a critical challenge, posing risks of SE separator penetration and short circuiting. Moreover, dynamic interfacial evolution during cycling leads to progressive contact degradation and increased interfacial impedance [114]. While recent modification strategies have achieved partial success in mitigating these issues, realizing long-term stability under practical operating conditions still demands integrated innovations in both material design and interface engineering. In contrast, carbon-based anodes offer more pragmatic engineering advantages (as discussed in the next section). These materials benefit from decades of industrial application in conventional liquid-electrolyte systems, with well-established manufacturing processes and clear cost-effectiveness. Their intrinsic layered or disordered structures allow for stable lithium intercalation/insertion and effectively buffer volume changes through engineered porosity, resulting in excellent cycling stability. Notably, carbonaceous materials exhibit superior physical compatibility with state-of-the-art SEs, significantly reducing interfacial side reactions compared to lithium metal [176]. Collectively, these features position carbon-based anodes as a more viable transitional solution for advancing SSBs from laboratory research to industrial-scale application.

Carbon-based anode active materials

Carbon-based components occupy an important position among AAMs because they possess high electronic conductivity, stable chemical properties, and are cost-effective [177,178]. Carbon-based AAMs in SSBs provide distinct benefits compared to lithium metal and alloy-type anodes when dealing with issues such as electro-/chemical side reactions, dendrite formation, and chemo-mechanical degradation at the interface [179]. For instance, graphite, which is commonly used as an anode in industrial applications, demonstrates high structural stability [28]. It experiences a volume expansion of less than 10 % during the lithiation process, which helps maintain the integrity of the anode structure [53]. In contrast, lithium metal and alloy AAMs undergo very large variations in volume, such as the expansion of Si by up to ~300 % [180]. This can cause them to physically detach from the SE, resulting in a decline in battery performance. Moreover, they tend to undergo unfavorable electro-/chemical reactions with SEs due to their high reactivity, leading to poor stability at the AAM|SE interface and loss of electrochemically active material. On the other hand, compared to lithium metal and alloy anodes, graphite has a lower surface energy, facilitating the formation of a stable SEI when exposed to SEs. This in turn decreases the likelihood of interfacial side reactions [181]. It is worth mentioning that graphite possesses excellent mechanical and tensile strength, high corrosion resistance, and a reasonably large specific surface area. These properties are advantageous for improving the cyclability of SSBs. Overall, carbon-based AAMs usually outperform lithium metal and alloy anodes in terms of structural and electrochemical stability, but they still face interfacial issues that affect the electrochemical performance in solid-state environments. Importantly, the inherently low theoretical specific capacity (graphite: 372 mAh g^{-1}) and relatively poor rate performance of these materials are significant obstacles that prevent SSBs from addressing the market needs for high energy and power devices [182].

Protective coatings

The application of a coating typically serves to avoid direct contact between the SE and the AAM. This has the effect of reducing the occurrence of side reactions, lowering interfacial resistance, and enhancing the rate performance and energy density of carbon-based AAMs [183,184]. Yang et al. developed a straightforward coating method that utilizes LiI to form a protective layer on the graphite surface [185]. The coated graphite delivered a higher specific discharge capacity (348 mAh g^{-1}) at 0.05C rate than the uncoated counterpart (248 mAh g^{-1}). Electrochemical impedance spectroscopy (EIS) and X-ray absorption spectroscopy (XAS) measurements revealed that the application of a LiI coating effectively reduces the interfacial resistance (by inhibiting the formation of decomposition products from sulfide SEs) and improves the power density of graphite. Yao and colleagues designed a composite coating of LiF and prelithiated graphite, placed between the Li_6PS_5Cl SE and the pristine graphite anode (Fig. 9a) [186]. The co-existence of LiF, C–F bonds, and prelithiated graphite in this unique coating promotes uniform lithium migration and compensates for active lithium loss, thereby significantly improving the cycling performance of SSBs.

Composites

Incorporating other materials into carbonaceous hosts is an effective strategy for designing advanced AAMs for SSBs. These composites can enhance ionic conductivity, strengthen the interfacial stability with SEs, and offer extra storage capabilities. However, further research is necessary to establish simple preparation methods and identify suitable combinations of carbonaceous materials and additives for realizing high-performance anodes that fulfill the targeted requirements [187]. Yan et al. developed a stable HC-lithium silicon alloy anode, in which a plastically deformable 3D ionically-electronically conductive network composed of lithium-rich phases ($Li_{15}Si_4$ and LiC_6) was formed. This network expanded the active area and alleviated stress concentration, ultimately improving the electrode's kinetics and mechanical stability. This design enabled long-term cycling under high loading and high current density while effectively suppressing lithium dendrite growth (Fig. 9b) [38]. Furthermore, Suzuki and coworkers applied a thin carbon

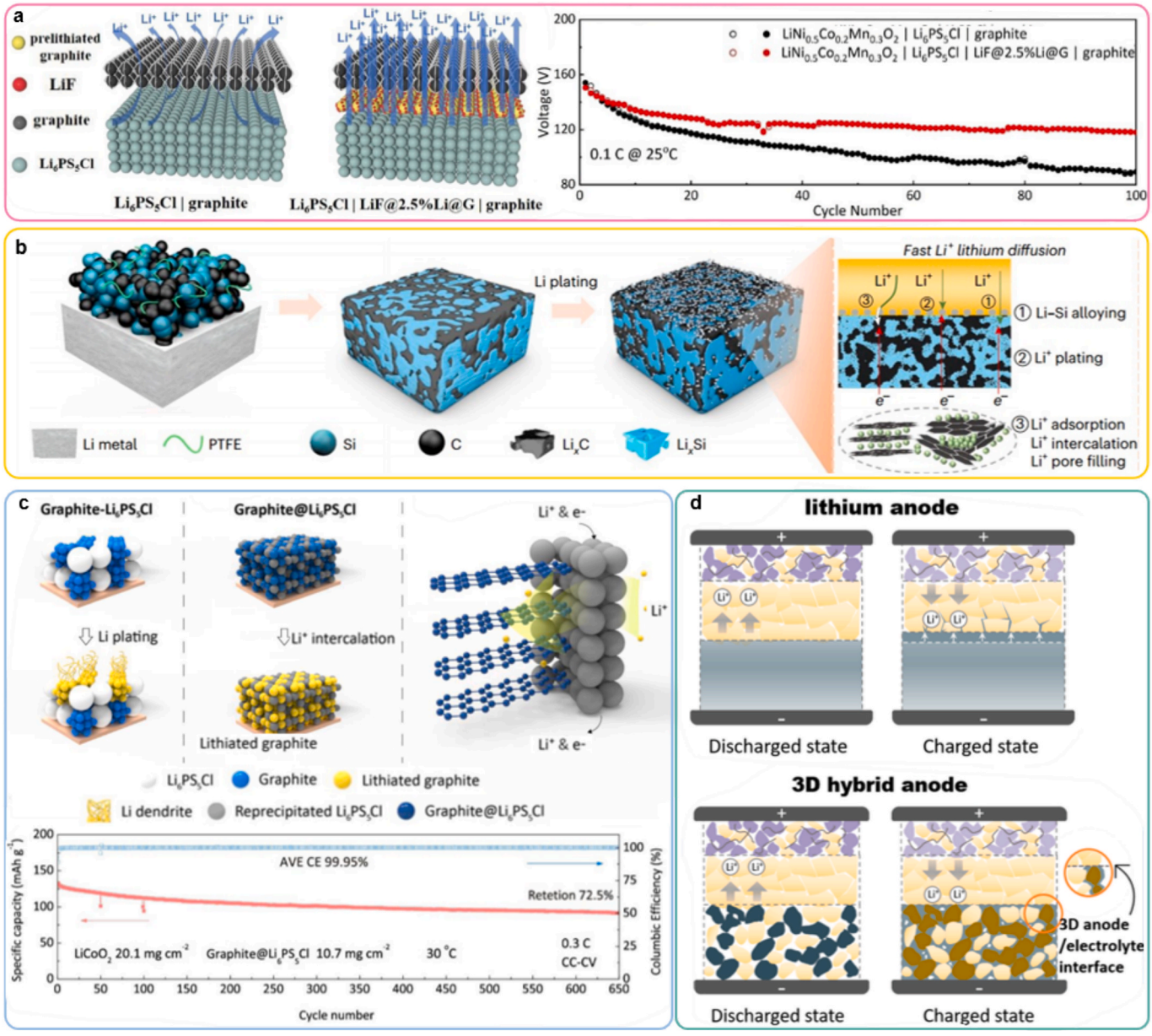

Fig. 9. Optimization strategies for carbon-based anodes. (a) Ion migration across the interface and cycling performance of graphite SSBs. Reproduced from ref. [186]. Copyright 2023, with permission from Wiley-VCH. (b) Schematic representations of HC-stabilized Li_xSi anodes. Reproduced from ref. [38]. Copyright 2023, with permission from Springer Nature. (c) Schematic representations of lithium plating on graphite-Li_6PS_5Cl, lithium intercalation into graphite@Li_6PS_5Cl, and the mixed electronically-ionically conductive (re-precipitated) Li_6PS_5Cl, as well as the cycling performance of a graphite@Li_6PS_5Cl| Li_6PS_5Cl|$LiCoO_2$ pouch cell. Reproduced from ref. [182]. Copyright 2023, with permission from Elsevier. (d) SSBs with lithium metal or 3D hybrid anodes. Reproduced from ref. [192]. Copyright 2021, with permission from American Chemical Society.

black layer to the CC, which effectively prevented battery short circuits [188]. Li et al. proposed a hybrid anode consisting of a 3D LiC_6 particle framework embedded with lithiophilic seeds, achieving uniform lithium dissolution/deposition [189].

Recent studies show that soft carbon is a viable AAM for SSBs. Soft carbon features small grains, large lattice spacings, low crystallinity, as well as a high specific surface area and porosity. Wang et al. designed an N- and S-doped soft carbon with multiple diffusion channels and expanded interlayer spacing [190]. Both the increased interlayer spacing and the heteroatom doping promote ion diffusion (rate capability), reduce the local current density within the anode, and suppress the growth of dendritic lithium. Aside from that, SSBs with $LiCoO_2$ (LCO) as cathode active material (CAM) and Li_6PS_5Cl as SE were shown to achieve a high areal capacity of 15 mAh cm^{-2}, a specific energy of 403 Wh kg^{-1}, and an excellent cycle life (13000 cycles). In addition, they prepared a soft carbon|$Li_{6.4}La_3Zr_{1.4}Ta_{0.6}O_{12}$ interface with a mixed conductive network and high Li^+ diffusion coefficient [191]. In this configuration, the nanoscale SE facilitates ion diffusion across the interface and prevents dendrite growth.

Structural optimization

Tailoring the morphology and structure of carbonaceous AAMs can yield some advantages, namely (i) increasing the contact area with SEs, thereby enhancing the efficiency of ion transport and reaction kinetics; (ii) reducing volume changes during cycling, thus effectively inhibiting damage to the anode structure and enhancing interfacial stability; and (iii) suppressing interfacial side reactions by smart structural design for

ensuring safe and reliable operation of SSBs [193].

Zhang et al. designed a core–shell microstructure of graphite@Li_6PS_5Cl with good structural stability and fast kinetics [182]. At 0.3C and 2.4 mAh cm^{-2}, SSBs with LCO cathode and graphite@Li_6PS_5Cl anode exhibited a high average CE of over 99.9 % and a capacity retention of ~ 73 % after 650 cycles at 30 ℃ (Fig. 9c). Xing et al. reported a 3D hybrid framework composed of lithiated graphite and Li_3PS_4 [192]. By evenly depositing additional lithium into the voids within the framework during battery operation, a 3D graphite-lithium hybrid anode was realized. Electrodes designed in this way can significantly mitigate issues of short-circuiting (Fig. 9d).

CVD is a commonly used technique for growing graphene sheets on metal substrates. Wei et al. have grown monolayer graphene directly onto Cu foil through CVD, resulting in a battery of total thickness 50 μm. This ultrathin battery demonstrates a maximum volumetric energy density of 10 Wh L^{-1} and a peak power density of 300 W L^{-1} [194]. To modulate the micropore properties and suppress unwanted reactions, Kaskel and coworkers developed carbide-derived carbon of high microporosity (specific surface area > 1500 m^2 g^{-1}) [195]. The well-defined micropores are capable of inhibiting SEI formation at the pore entrances and within accessible pores. This reduces capacity loss during the first cycle and ensures long-term stability of lithium deposited within the pores. Therefore, porous host materials provide new opportunities for optimizing SSB performance and commercial applications. However, the existence of micropores also creates electrochemically inactive regions, potentially reducing the volumetric energy density.

Conclusion

While carbonaceous anodes have become a viable option in SSB development due to their mature processing foundation and stable cycling performance, the intrinsic energy storage capacity is approaching its theoretical limit. The inherent lithium storage mechanism of graphite-based materials restricts the capacity enhancement potential, with even optimized disordered carbon structures struggling to surpass the 500 mAh g^{-1} threshold. This energy density bottleneck becomes increasingly prominent in high-end applications, such as electric vehicles and grid-scale storage, driving research interests toward more promising alloy-based systems, which will be discussed in the following section. Alloy-type anode active materials, benefiting from multi-electron reaction mechanisms, offer theoretical specific capacities 2–4 times higher than that of graphite, presenting a viable route to overcome energy density limitations. Moreover, alloy systems are capable of confining volumetric changes within reasonable ranges through nanostructuring [196]. Recent studies have demonstrated that prelithiated silicon anodes can be cycled stably over 200 cycles, establishing a practical pathway for next-generation SSBs [25].

Alloy-based anode active materials

Alloys based on Si, Sn, or Al as AAMs offer high theoretical specific capacities stemming from de-/alloying reactions with lithium, potentially significantly enhancing the energy density of SSBs (Table 2) [197–199]. Importantly, alloys are generally made of abundant materials, non-toxic, and of great significance for industrial applications in the field of batteries [200,201]. However, they often undergo large volumetric and structural variations upon de-/lithiation, which may lead to anode degradation and/or failure [202,203]. Jeong et al. investigated the electrochemical alloying and dealloying behavior of various candidate alloy foil anodes in SSBs using Li_6PS_5Cl as SE. They found that lithium entrapment within the foils during delithiation is the primary reason for the low CE of most materials, with indium exhibiting superior CE due to a unique delithiation front evolution, where the highly diffusive Li-In phase remains at the SE interface [204]. Additionally, they reported the synthesis of In and Sn foil structures with bicontinuous porosity, demonstrating that porous In exhibits excellent electrochemical performance in SSBs [205]. Yanev et al. evaluated the suitability of Li-In as a counter electrode in sulfide-based SSBs (dual-electrode half-cell configuration) and proposed an improved manufacturing scheme to optimize its performance [206]. To elucidate the correlation between structure and reactivity, Wan et al. employed *in situ* electrochemical atomic force microscopy and quantitatively analyzed the surface area and volume of wrinkled structures, revealing a "breathing" phenomenon during the cycling behavior of Li-In alloying/dealloying reactions [207]. Moreover, Lu et al. employed a lithium alloy anode as a model system to quantify the kinetic evolution and transition of lithium from alloying reactions to metal deposition in SSBs, identifying carrier transitions from lithium atoms to lithium vacancies during lithiation [208].

In recent years, Si has garnered significant interest and is widely used in advanced LIBs with customized liquid electrolytes. There are several primary factors to take into account: (i) its suitable lithiation potential (~0.4 V vs. Li^+/Li), which is lower than that of other alloys and further helps avoid the risk of lithium plating and dendrite growth; and (ii) its high theoretical specific capacity (3590 mAh g^{-1} for $Li_{3.75}Si$), which is similar to that of lithium metal and about ten times higher than that of graphite [210,211]. Importantly, in solid-state environments, Si anodes are expected to provide higher energy density than lithium metal anodes. Considering the cost and preparation process, Si anodes have great potential for application in SSBs [212]. While lithium metal anodes attract great attention for their ultrahigh capacity, silicon exhibits unique advantages in SSBs that align more closely with practical

Table 2
Properties of different lithium alloys [209].

Material	Lithiated phase (s)	x(Li)	Volume expansion (%)	Type	Electrode potential (V vs. Li^+/Li)	Theoretical specific capacity (mAh g^{-1})
Magnesium	Li_xMg	0–1.95	0–125	Solid solution	0.03	0–2150
Indium	LiIn	1	105	Solid solution, Intermetallic compound	0.62	220
Zinc	Li_2Zn_5	0.4	39	Solid solution, Intermetallic compound	0.49	164
	$LiZn_2$	0.5	49		0.256	205
	Li_2Zn_3	0.67	65		0.249	273
	LiZn	1	98		0.157	410
Aluminum	LiAl	1	90	Solid solution, Intermetallic compound	0.38	993
Silicon	$Li_{3.75}Si$	3.75	280	Intermetallic compound	0.4	3590
Tin	$Li_{0.4}Sn$	0.4	22	Intermetallic compound	0.76	90
	$Li_{0.7}Sn$	0.7	39		0.66	158
	$Li_{2.33}Sn$	2.33	129		0.53	527
	$Li_{2.63}Sn$	2.63	146		0.485	594
	$Li_{3.5}Sn$	3.5	194		0.42	790
	$Li_{4.4}Sn$	4.4	244		0.38	993

requirements. Although the theoretical specific capacity of silicon is slightly lower than that of lithium metal, its superior volumetric energy density plays a more critical role in electrode design [211]. Furthermore, its abundance in the Earth's crust ensures lower raw material cost and greater supply chain stability, while mature fabrication techniques demonstrate higher compatibility with SSB manufacturing processes [196]. This synergy of material accessibility, process compatibility, and system-level safety positions silicon anodes as a balanced solution in terms of performance, cost, and industrial scalability [213]. The present studies have concentrated on the utilization of structural, interfacial, and component engineering approaches to improve the electrochemical performance of alloy-type anodes in SSBs [214]. Ping et al. were the first to report a 1 μm-thick solid-state silicon anode as a viable alternative to lithium metal in SSBs. The Si electrode, combined with a garnet SE, exhibited a high specific discharge capacity of 2685 mAh g^{-1} and an excellent ICE of ~83 % [196].

Structural engineering

This strategy is often employed to enhance the performance of alloy anodes, aiming at mitigating issues associated with structural instability due to large volume changes [215]. The approach involves tailoring the dimensions of the alloy structures (nanowires or thin films) for controlling the physical contact area with the SE and preparing buffer space within the material (porous or core–shell structures) to accommodate the volume expansion/contraction, thereby improving the overall anode stability and prolonging the lifespan of SSBs [216]. Wan et al. fabricated a 3D porous zinc layer on the surface of $Li_{6.4}La_3Zr_{1.4}Ta_{0.6}O_{12}$ using magnetron sputtering. They incorporated lithium metal into the zinc layer to create a 3D lithium-zinc alloy at the $Li_{6.4}La_3Zr_{1.4}Ta_{0.6}O_{12}$|Li interface. The latter 3D alloy effectively suppressed the volume expansion at the interface between the SE and the lithium metal [217]. Kaskel and colleagues prepared 2D columnar Si as an anode in SSBs using Li_6PS_5Cl as SE. In this configuration, the SE penetration is limited to the gaps between the individual Si pillars, with intimate contact only established at the top surface of each pillar. As a result, the interfacial contact area is reduced, which helps suppress side reactions and leads to the formation of a 2D (lateral) SEI. Meanwhile, the area between the Si pillars can serve as buffer space to mitigate the volume expansion of the anode. Based on these benefits, SSBs with $LiNi_{0.9}Co_{0.05}Mn_{0.05}O_2$ as CAM offer a high areal capacity of 3.5 mAh cm^{-2} and exhibit stable cycling with a capacity retention of ~ 82 % after 100 cycles [216]. By using micro-Si as AAM, Meng's group successfully developed almost pure Si (99.9 %) anodes (Fig. 10a) [39]. They utilized the passivation effect to construct a stable Si|Li_6PS_5Cl interface, exhibiting promising electrochemical performance. Specifically, the cell was found to achieve a capacity retention of ~ 80 % after 500 cycles and an average CE of > 99.9 %. Subsequently, An et al. discovered that polyvinylidene fluoride can be substituted with the water-based binder polyacrylic acid, which allows for the development of sustainable and eco-friendly Si anodes for SSB application [218].

Composites

Combining alloy-based AAMs with other materials is an effective strategy that may not only mitigate the volumetric expansion during cycling but also enhance the ionic conductivity of the electrode [219]. Additionally, the inherent mechanical reinforcement of composite materials further strengthens the structural stability. Zhang et al. embedded Si nanoparticles into micrometer-sized MOF-derived carbon hosts, effectively accommodating changes of Si during cycling while providing sufficient charge transfer pathways [220]. The Si@MOF anode exhibited good interfacial stability with a composite polymer electrolyte for over 1200 h and achieved a high areal capacity of 3 mAh cm^{-2} (Fig. 10b). Ham et al. employed a pre-lithiation strategy to enhance both the ICE and the conductivity of Si anodes. This pre-lithiation approach resulted in a 15 % improvement in capacity retention after 1000 cycles compared to pure Si [221]. Carbonaceous materials are often used as additives due to their unique mechanical properties [222,223]. Taeseup and colleagues reported on the use of Si nanoparticles embedded in carbon nanofibers (Si/CNF) as anode material for SSBs [224]. Embedding Si nanoparticles in CNF allows for easy stress relaxation and abundant electronic pathways. The protective function of the conductive matrix can reduce resistance in SSBs. Coal tar pitch, a by-product of the coal industry, possesses excellent properties in the form of mixed conducting, amorphous carbon generated through pyrolysis. Dunlap et al. prepared a Si-carbon composite by pyrolyzing coal tar pitch to form an active soft carbon matrix. The prepared electrode delivered a high capacity and showed good electrochemical performance [225].

The selection of alloy components, the distribution of alloy phases, and interface engineering between the composite and the SE are crucial for enhancing the electrochemical properties. Kim et al. prepared Li_3PS_4 glass + Li-Si alloy and Li_3N + LiF + Li-Si alloy composites, combining Li_3N and LiF to leverage the advantages of both materials for suppressing lithium dendrite growth [226]. Zhang et al. developed a Si/$Li_{21}Si_5$ composite anode, where $Li_{21}Si_5$ particles were uniformly distributed among the Si particles, serving as a soft buffer layer for Si and forming a conductive network in the anode, thereby preventing dendrite formation [227]. Yersak et al. also developed and characterized a Si-Ti-Ni ternary alloy, achieving high specific capacities [228]. To further enhance kinetics, Mo et al. introduced liquid gallium (Ga) into a representative antimony (Sb) anode, which, through *in situ* generation, stimulated the lithiation/delithiation activity, achieving excellent rate capability and cycling performance [229]. Furthermore, establishing highly percolating transport pathways for electrons and ions in the anode is crucial for performance enhancements. Yang et al. constructed a dual-conductive framework by partially dealloying the Li-Mg anode on a garnet-type SE [230]. Upon delithiation, the alloy transforms into a lithium-deficient material with a porous framework while retaining strong interfacial contact with the SE. The presence of residual lithium in the alloy allows the skeleton to serve as pathways for both ions and electrons. Superior to previous surface treatment methods, even when a large quantity of lithium is stripped, the dual-conductive solid framework can serve as an effective host without interfacial degradation or volume collapse. In addition, He et al. doped strontium (Sr) into the lithium anode, creating a bifunctional layer having lithiophilic and lithium-repelling characteristics by enriching Li-Sr/SrO-doped Li_2O at the interface [231]. This approach differs from previous methods that formed lithiophilic interlayers using metal/metal oxide coatings on garnet or alloy-type anodes. The optimized Li-Sr|garnet|Li-Sr cell achieved a critical current density of 1.3 mA cm^{-2} and successfully cycled for 1000 times at 0.5 mA cm^{-2}.

Electrocatalysis is typically limited to dynamic liquid–solid and gas–solid interfaces and is rarely applicable to solid-state reactions. Zhou et al. used heteroatom doping, specifically boron in silicon and sulfur in phosphorus, to catalyze the electrochemical lithiation reactions in SSB materials, significantly improving the rate performance of boron-doped silicon and sulfur-doped black/red phosphorus anodes [232]. Among them, the red phosphorus exhibits unique advantages. It not only has a high theoretical specific capacity (2596 mAh g^{-1}) but also significant natural abundance (0.118 %) and a relatively high working potential (~0.97 V vs. Li^+/Li). However, stable cycling of red phosphorus-based anodes in sulfide SSBs has yet to be achieved. Tang and colleagues loaded sub-nanometer red phosphorus clusters into the micropores of activated carbon [233]. Due to the moderate lithiation potential and fast ion diffusion, this composite anode can sustain high current densities without forming lithium dendrites in symmetrical cells.

In fact, most sulfide-based SSBs use Li-In alloys as AAM. However, the effect of different lithium concentrations in these alloy anodes on the electrochemical performance remains unclear, and the reaction kinetics between Li and In have not yet been studied in detail. Wang et al. systematically investigated the effect of different lithium concentrations in

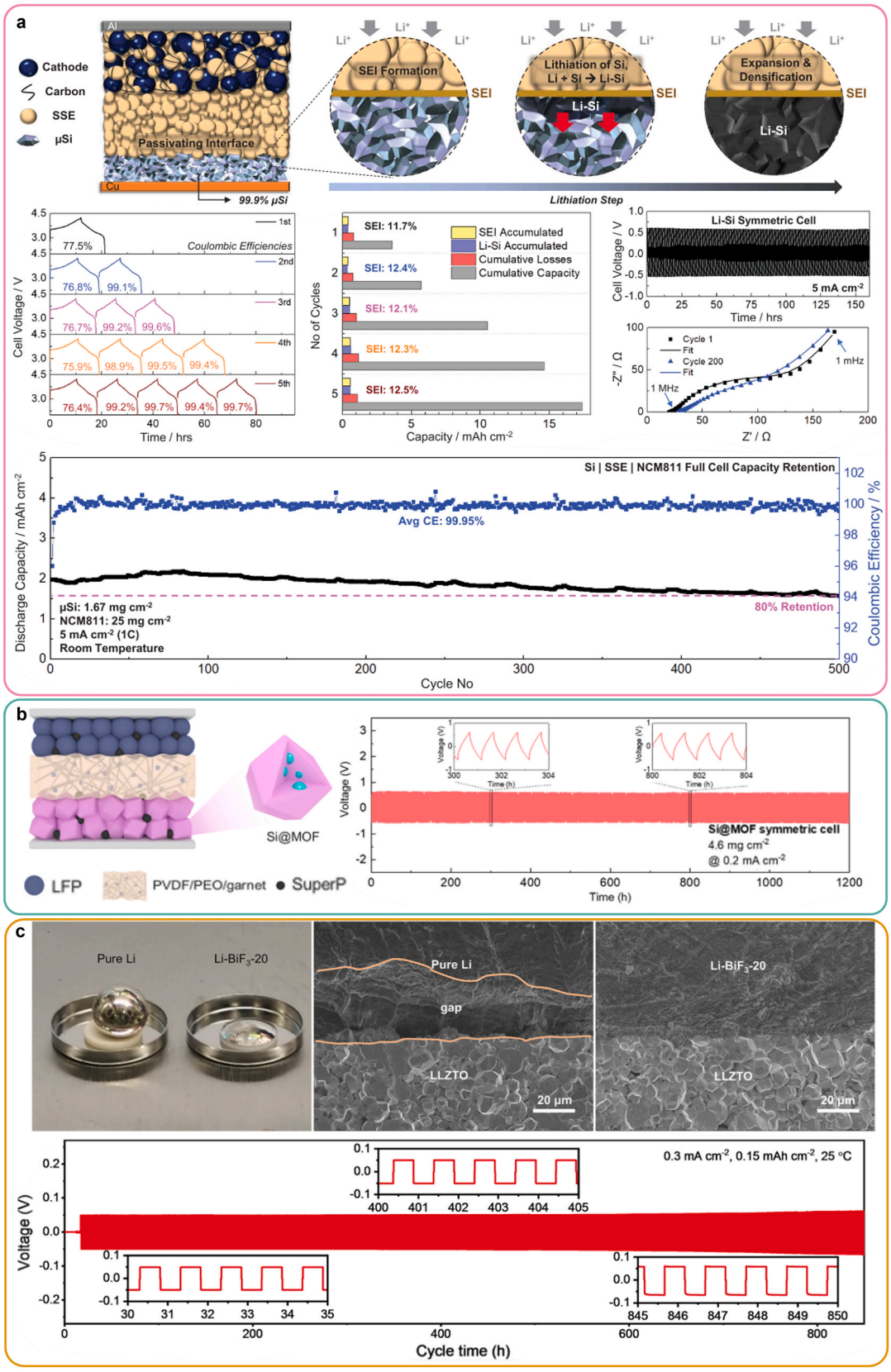

Fig. 10. Design strategies for alloy-based anodes. (a) Schematic of a μSi anode in SSBs, quantification of SEI growth, and cycle life at room temperature. Reproduced from ref. [39]. Copyright 2021, with permission from American Association for the Advancement of Science. (b) Schematic illustration of SSBs using bare Si or Si@MOF as anode and voltage profiles of a Si@MOF symmetric cell cycled at 0.2 mA cm^{-2} for 1200 h. Reproduced from ref. [220]. Copyright 2022, with permission from American Chemical Society. (c) Photographs of molten lithium on different substrates, cross-sectional SEM images of Li|$Li_{6.4}La_3Zr_{1.4}Ta_{0.6}O_{12}$ and Li-BiF_3|$Li_{6.4}La_3Zr_{1.4}Ta_{0.6}O_{12}$ interfaces, and cycling stability of a Li-BiF_3|$Li_{6.4}La_3Zr_{1.4}Ta_{0.6}O_{12}$|Li-$BiF_3$ cell. Reproduced from ref. [239]. Copyright 2023, with permission from Elsevier.

Li-In alloy anodes on the cyclability of sulfide-based SSBs. Their findings indicated that the anode containing 1 wt% lithium exhibits the best performance [234]. Hänsel et al. revealed the fundamental electrochemical and mechanical behavior of Li-In and Li-Sn alloys with different lithium stoichiometries in sulfide-based SSBs [235]. Gao et al. developed a lithium-rich Li-In anode, in which the $Li_{13}In_3$ alloy acted as a 3D framework for accommodating lithium and mitigating volume changes, while the residual lithium served as a lithium source, shuttling between anode and cathode during cycling [236].

Employing conductive coating strategies not only boosts the ion mobility at the interface but also partially alleviates the interfacial stress caused by volumetric changes during de-/lithiation [237]. They can also mitigate interfacial tension caused by the changes in volume of alloy-type anodes. Ci's team introduced a coating of $LiAlO_2$ on the surface of Si particles [238]. The $LiAlO_2$ layer, with reasonably high ionic conductivity and mechanical strength, promoted the diffusion of lithium between the Si particles, resulting in good cycling performance and enhanced rate capability. Li et al. devised a high-performance Li-BiF_3 composite system, incorporating a continuous ionically conductive phase achieved via conversion reaction between BiF_3 powder and molten lithium [239]. This composite boasts an *in situ* generated Li_3Bi phase, which facilitates ion migration to the interface, effectively compensating for lithium depletion during stripping (maintaining intimate interfacial contact and mitigating void formation). Furthermore, the presence of Bi softens the bonding among the lithium atoms, resulting in a decrease in surface tension. Thanks to these advantageous traits, Li-BiF_3|$Li_{6.4}La_3Zr_{1.4}Ta_{0.6}O_{12}$|Li-$BiF_3$ cells display a low interfacial resistance of 7.4 Ω cm^2 and sustain long-term cycling stability for over 850 h at 0.3 mA cm^{-2} (Fig. 10c).

Conclusion

The continuous volume expansion/contraction of alloy-type materials during charging/discharging leads to poor interfacial contact between the electrode and the SE. Current modification strategies primarily focus on addressing superficial issues, lacking comprehensive analysis linking atomic-scale structural evolution to macroscopic performance degradation. As a result, many proposed solutions merely alleviate the symptoms without tackling the root causes. To overcome these challenges, future research should prioritize the development of adaptive buffer structures and interfacial modification layers that combine chemical inertness with dynamic self-healing properties. Furthermore, it is essential to unravel the key factors driving structural degradation during battery operation and clarify their coupling mechanisms with the electrochemical behavior. Such insights will be critical to bridging the gap between laboratory research and industrial-scale

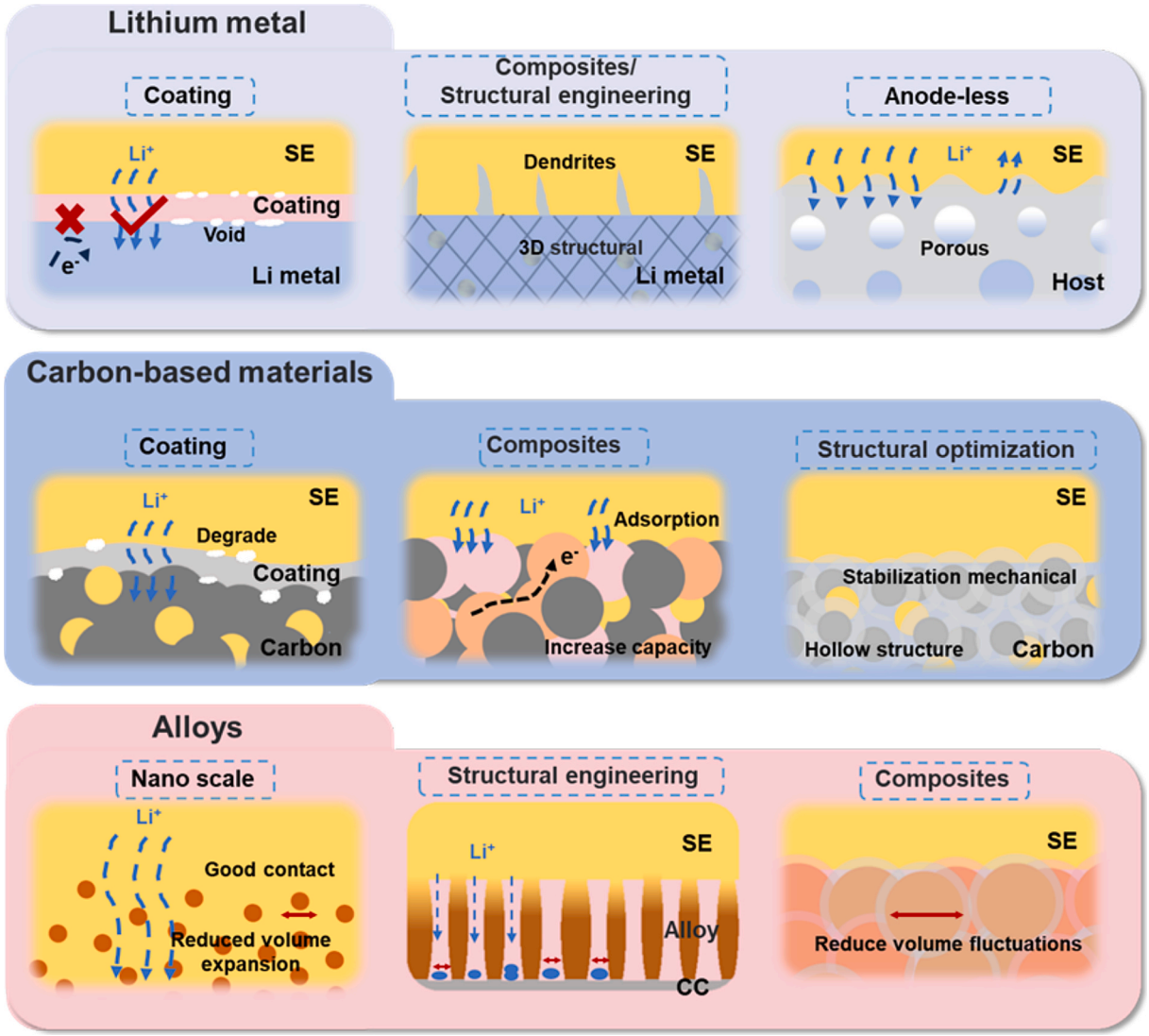

Fig. 11. Summary of optimization strategies for SSB anodes.

implementation.

Summary and outlook

Summary

Research on AAMs in the field of SSBs is characterized by diversity and dynamics. From this perspective, we provide a concise overview of viable anodes and highlight the main challenges they encounter, with a focus on the progress made in compositional and structural engineering (Fig. 11). While recent research has made significant advancements, numerous pressing concerns need to be addressed to effectively utilize the findings.

Lithium metal, due to its high reactivity and large theoretical specific capacity, has become a popular choice for SSBs. However, lithium metal anodes undergo major volume changes during plating and stripping, leading to uneven SEI formation, which can exacerbate dendrite growth, shorten battery life, and pose safety risks [20]. Additionally, its high reactivity and the need for special environments during processing increase production costs, limiting commercial applications. To overcome these challenges, constructing an interfacial, protective layer has proven to be an effective strategy [240]. Currently, a variety of inorganic and organic materials, including lithium-containing and lithium-free compounds, have been proposed for interfacial protection. The latter often transform into lithium-containing compounds of reasonably high ionic conductivity after *in situ* reaction with lithium. The criteria for an ideal interfacial layer should include four essential characteristics: high ionic conductivity, good wettability with the SE/lithium, high electrochemical stability, and low electronic conductivity. Future research in this direction should focus on developing intermediate layers with strong bonding to both the lithium and the SE particles, thereby maintaining intimate contact. Modulating the structure and composition of lithium metal is another promising approach to achieving stable lithium deposition/stripping. By designing lithium with unique morphologies and composites with other materials, the ion diffusion dynamics at the interface can be significantly enhanced, leading to more uniform lithium deposition and mitigated dendrite growth. Anode-less configurations represent a milestone in SSB development. From a practical perspective, reducing lithium metal usage and simplifying battery assembly during manufacturing offer significant advantages. However, the ICE and reversibility of lithium plating/stripping upon cycling are crucial for the practical energy density and cycle life. Modifications to the CC, including the selection of suitable host structures combined with lithiophilic coatings, have proven viable options for enhancing reversibility towards achieving 100 % CE. While lithiophilic coatings or protective layers on CCs have been shown to improve the stability of anode-less SSBs, extensive use of these measures can significantly reduce energy density, diminishing the advantages of such batteries [30].

Carbonaceous materials with their excellent mechanical stability as well as high electronic conductivity and chemical/electrochemical stability are regarded as important AAMs. They not only serve directly as the negative electrode for SSBs but also function as core components in composite anodes. However, their slow reaction kinetics, low ICE, and modest capacity pose bottlenecks for further development. To address these challenges, current optimization strategies primarily focus on structural tailoring, surface coating, and composites with other materials [193,195]. By coating carbonaceous materials, the interlayer spacing can be effectively increased, facilitating ion transport, extending cycle life, and reducing charge-transfer resistance at the electrode|SE interface. It should be noted though that insufficient bonding strength between the coating and the carbon-based matrix may lead to detachment, weakening the overall effect. Additionally, structural optimization of carbon-based materials effectively reduces their specific surface area, thereby inhibiting parasitic effects and enhancing ICE [241].

Overall, these strategies represent the synergistic application of multiple materials and modification methods to yield properties superior to those of the base carbonaceous materials. Notably, while carbon-based materials hold great potential for application in SSBs, their performance limitations still restrict widespread adoption. Therefore, future research should delve deeper into the potential of different kinds of carbonaceous materials, driving their broader application in the SSB field through continuous innovation and optimization, ultimately maximizing their value.

Alloys with their high reversible capacity, suitable operating potential, and favorable transport properties have been extensively researched as primary anodes for the next generation of high-energy–density batteries. However, severe volume changes during charging and discharging limit their cycle life. Currently, nanostructure design, coating strategies, morphology control, and compositing with other materials have emerged as mainstream solutions to shorten diffusion path lengths, enhance conductivity, and accommodate volume variations [216,242]. Nanosizing alloy-based materials usually positively affects ion diffusion and electron conduction, mitigating performance degradation. The construction of alloy composites can improve conductivity, stabilize the electrode structure, and provide a protective layer through compositing, thereby alleviating volume changes and forming a stable anode|SE interface to maintain structural stability during cycling. While there are some studies on the application of alloy-based anodes in SSBs, most of them focus on regulating the ionic conductivity of SEs and designing electrode structures, with limited reports on electrode|SE interfaces and insufficient understanding of failure mechanisms. Additionally, issues related to the cost of nanostructured materials and the packing density of the anodes have not been thoroughly addressed. Future research should delve deeper into the interface compatibility between alloy-based anodes and SEs to guide the development of advanced SSBs.

Outlook

Below are some approaches and suggestions for future research (Fig. 12). In the commercialization process, lithium metal anodes are considered the cornerstone for achieving high-performance SSBs due to their favorable characteristics of high theoretical specific capacity and low electrochemical potential. However, the current challenges lie in the growth of lithium dendrites during battery operation and accompanied safety concerns. A more revolutionary approach involves developing liquid metal-type anodes, where dendrite formation can be mitigated through dissolution, enabling dendrite-free operation and ultra-long cycle life. The application of this technology necessitates novel battery designs and the development of protective layers to shield the SE particles from the corrosive liquid. Additionally, innovative methods such as magnetic lithium and gradient composite lithium anodes have led to promising performances in reducing interfacial resistance and inhibiting dendrite formation and growth. Simultaneously, thorough understanding of the interactions between (artificial) protective layers and lithium metal and/or solvated lithium ions remains to be acquired. This often necessitates a synergistic combination of experiments, simulations, and theoretical calculations, along with continuous compositional and structural optimization of coatings through various preparation methods, particularly under high current density or high capacity testing conditions, to ensure proper protection of the lithium metal. Moreover, drawing on knowledge from other disciplines should be strongly encouraged to provide deeper insights into the complex lithium metal interface, such as stress accumulation/release and thermal effects during plating/stripping. Regarding anode-less configurations, numerous improvement strategies have been successfully demonstrated at the laboratory level. Nevertheless, direct translation to practical batteries appears highly challenging in most cases. While laboratory-scale strategies are instrumental in addressing mechanical issues for commercial deployment, rational application technologies are crucial for realizing these solutions in scaled-up battery systems. In the future,

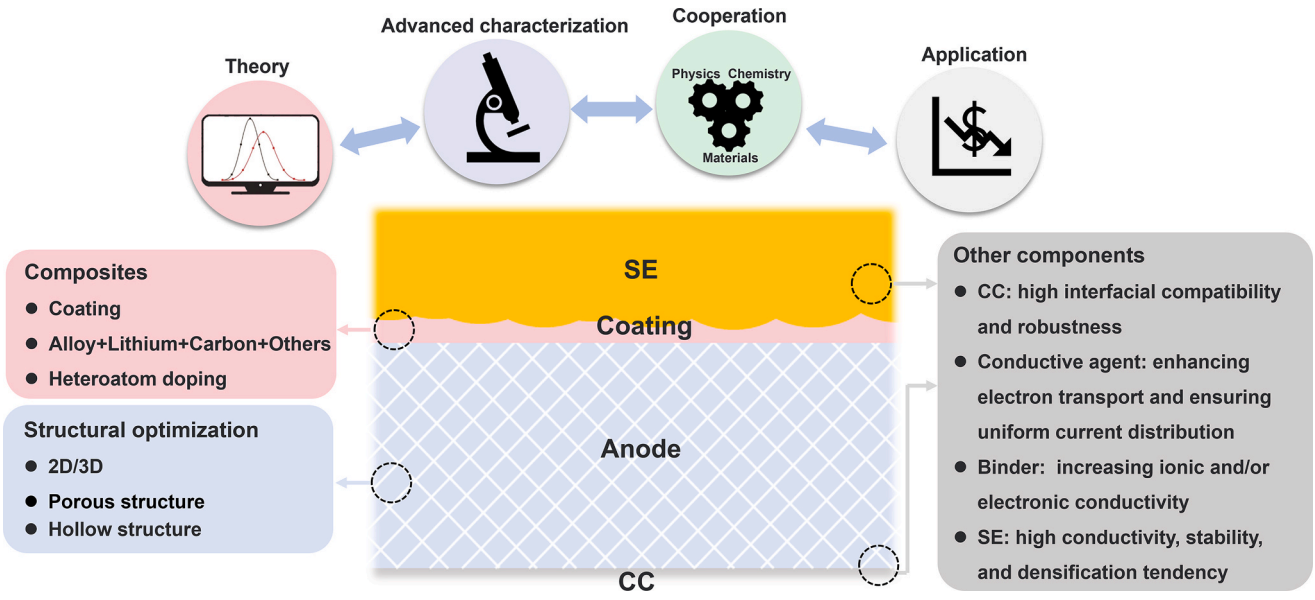

Fig. 12. Future perspectives of SSB anodes.

greater attention should be paid to this aspect in laboratory-scale developments. Exploring fundamental mechanisms through multiscale analysis, in-depth electrochemical testing, and actual manufacturing will pave the way for the commercialization of anode-less SSBs.

The application of carbon-based anode materials in the field of SSB faces numerous challenges such as limited lithium storage capacity, which significantly constrain their potential as primary anode materials for high-performance SSBs. Nevertheless, it is the high conductivity, excellent cycling stability, and structural freedom exhibited by carbon-based electrode materials that enable them to serve as additives or composite components, significantly enhancing the overall anode performance. For instance, by tailoring the particle size, pore structure, and surface chemistry of carbonaceous materials, one can optimize composite effects with active lithium storage materials like Si or Ti-based alloys, facilitating rapid ion transport and uniform distribution, thereby effectively mitigating volume variations and prolonging the battery's cycle life. Furthermore, research into the compatibility of carbon-based anodes with other materials will emerge as a crucial direction in the field of AAMs in the future. This not only necessitates a profound understanding of the behavior of carbonaceous materials in various composite systems but also calls for exploring ways to further strengthen the interactions between active and inactive materials and SEs through interface engineering, surface modification, and other methods. This kind of research will strongly contribute to enhancing the performance of SSBs and has the potential to provide theoretical foundations and technical support for the development of novel composite anodes.

In the journey towards commercializing SSB technology, alloy-based anodes are regarded as crucial components for enhancing the performance. However, the significant volume changes during alloying and dealloying and the challenge of maintaining interfacial stability pose key challenges that need to be addressed. Despite the superior performance of various alloy-based anodes demonstrated in the laboratory, translating them into commercial-grade products requires overcoming several hurdles, including manufacturing cost control, standardization of production processes, and verification of long-term stability under high energy density conditions. Consequently, future research should concentrate on the transformation pathways (from laboratory to industrial applications), accelerating the research and validation of scalable production technologies to achieve early breakthroughs for alloy anodes in the field of SSBs. Additionally, delving into the behavioral patterns and conduction mechanisms at the AAM|SE interface will provide guidance for future research on alloy-based SSBs. On this basis, it is imperative to strengthen the theoretical calculations for alloy-type anode applications and their compatibility with SEs, complemented by experimental validation, to ensure close integration of theory and practice. Furthermore, the active exploration and development of more advanced testing technologies and computational models are essential for thoroughly analyzing the composition and dynamic evolution of the AAM|SE interface, laying the foundation for the continuous optimization of the alloy anode technology.

A battery is a complex system where enhancements in single parameters may potentially exert a negative impact on other metrics. While research on AAMs has led to major performance improvements, the engineering of electrode structures and battery configurations should not be overlooked. The interface issues between SEs and AAMs remain a central focus of current research. Among them, the low shear modulus, low mechanical strength, space-charge layer effect, and low stability (non-uniform SEI formation) of SEs are the primary causes of lithium dendrite growth. The main directions for SE modification involve reducing internal porosity, increasing relative density, and enhancing electrochemical stability [104,243]. Improving ionic conductivity, ion transport at the electrode/SE interface, and mechanical properties relies heavily on optimizing the atomic-level structure of the materials. Advanced CCs are typically characterized by high electrochemical stability and conductivity, high mechanical strength, and low cost [244]. Furthermore, conductive additives can potentially have detrimental effects on the SE. For instance, in SSBs, carbon additives can react with sulfide SEs, increasing electrode resistance and decreasing electrochemical activity. Conductive agents may not be necessary if the active material particles possess sufficiently high electronic conductivity and form a percolating network. Therefore, developing materials with high chemical stability and electronic conductivity represents a promising direction for future developments. Binders also play a vital role by connecting active material, conductive agent, SE, and CC. They not only mitigate volume changes during cycling and alleviate cracking but also form ion channels to accelerate lithium migration. Additionally, some binders rich in nitrogen- and oxygen-containing functional groups can enhance ion mobility. However, controlling the amount of binder is challenging; a small fraction may not effectively form continuous transport channels, while excess can adversely affect ion/electron transport. Thus, new methods need to be developed to achieve high electronic and ionic conductivity in high-loading anodes and/or to strictly control the content of polymeric binder. With the advent of big

data, material genomics and data-driven machine learning techniques are being applied to battery materials R&D. Future research should prioritize the development of intelligent machine learning algorithms to facilitate the discovery and design of high-performance AAMs through high-throughput screening and data analysis while reducing experimental costs. Advanced characterization techniques with multiscale and high-resolution capabilities such as cryogenic electron microscopy, synchrotron-based X-ray diffraction, or neutron diffraction can track the structural and compositional evolution of anode materials and the SEI during electrochemical cycling. The integration of these characterization methods with robust theoretical predictions is conducive to revealing critical influencing factors, guiding the design of AAMs and thereby accelerating the development of novel materials.

In summary, the research on SSBs can be seen as a kind of systematic engineering, which requires considering the development of battery cells as a whole rather than focusing on a single component. It is foreseeable that with the unremitting efforts of scientists and engineers worldwide, the commercialization of safe and energy-dense SSBs will soon become a reality.

CRediT authorship contribution statement

Zhenqi Song: Writing – review & editing, Writing – original draft, Visualization, Investigation, Formal analysis. **Yanjiao Ma:** Writing – review & editing, Writing – original draft, Validation, Investigation, Funding acquisition. **Xinbing Cheng:** Writing – review & editing, Methodology, Investigation. **Zhi Zhu:** Writing – review & editing, Methodology, Investigation. **Yiren Zhong:** Writing – review & editing, Methodology, Investigation. **Jiarui He:** Writing – review & editing, Methodology, Investigation. **Tao Wang:** Writing – review & editing, Methodology, Investigation. **Dinghao Xu:** Writing – review & editing, Methodology, Investigation. **Qianyu Zhang:** Writing – review & editing, Methodology, Investigation. **Kenneth I. Ozoemena:** Writing – review & editing, Methodology, Investigation. **Torsten Brezesinski:** Writing – review & editing, Writing – original draft, Formal analysis. **Yuan Ma:** Writing – review & editing, Writing – original draft, Supervision, Methodology, Funding acquisition, Formal analysis, Conceptualization. **Stefano Passerini:** Writing – review & editing, Writing – original draft, Investigation. **Yuping Wu:** Writing – review & editing, Supervision, Funding acquisition.

Declaration of competing interest

The authors declare that they have no known competing financial interests or personal relationships that could have appeared to influence the work reported in this paper.

Acknowledgments

This work was supported by the project on Natural Science Foundation of China (Key Project of 52131306) and Carbon Emission Peak and Neutrality of Jiangsu Province (no.BE2022031-4) and by research start-up funds from Southeast University (RF1028624081), Nanjing Normal University (184080H201B41), and the Big Data Computing Center of Southeast University. S. P. acknowledges the support from the Austrian Institute of Technology basic funding.

Data availability

Data will be made available on request.

References

[1] S. Kalnaus, et al., Science 381 (2023) 1300, https://doi.org/10.1126/science.abg5998.
[2] K.J. Griffith, et al., Nature 559 (2018) 556–563, https://doi.org/10.1038/s41586-018-0347-0.
[3] H. Wan, et al., Nature 623 (2023) 739–744, https://doi.org/10.1038/s41586-023-06653-w.
[4] L. Ye, et al., Nature 593 (2021) 218–222, https://doi.org/10.1038/s41586-021-03486-3.
[5] Z. Ning, et al., Nature 618 (2023) 287–293, https://doi.org/10.1038/s41586-023-05970-4.
[6] J. Janek, et al., Nat. Energy 8 (2023) 230–240, https://doi.org/10.1038/s41560-023-01208-9.
[7] M.J. Wang, et al., Joule 5 (2021) 1371–1390, https://doi.org/10.1016/j.joule.2021.04.001.
[8] L. Sun, et al., Energy Storage Mater. 46 (2022) 482–502, https://doi.org/10.1016/j.ensm.2022.01.042.
[9] Y. Ma, et al., ACS Nano 16 (2022) 18682–18694, https://doi.org/10.1021/acsnano.2c07314.
[10] A. Masias, et al., ACS Energy Lett. 6 (2021) 621–630, https://doi.org/10.1021/acsenergylett.0c02584.
[11] Z. Bi, et al., Energy Mater. 2 (2022) 200011, https://doi.org/10.20517/energymater.2022.07.
[12] D. Wu, et al., Prog. Mater Sci. 139 (2023) 101182, https://doi.org/10.1016/j.pmatsci.2023.101182.
[13] Solid Power completes battery pilot production line. https://www.electrive.com/2022/06/07/solid-power-completes-first-pilot-production-line/, 2022 (accessed 13 September 2024).
[14] A.M. Nolan, et al., Joule 2 (2018) 2016–2046, https://doi.org/10.1016/j.joule.2018.08.017.
[15] Y. Ma, et al., Adv. Funct. Mater. 32 (2022), https://doi.org/10.1002/adfm.202111829.
[16] Y. Ma, et al., Chem. Mater. 36 (2024) 2588–2598, https://doi.org/10.1021/acs.chemmater.4c00301.
[17] Y. Zhang, et al., Angew. Chem. Int. Ed. 59 (2020) 7797–7802, https://doi.org/10.1002/anie.202000023.
[18] C. Lee, et al., ACS Energy Lett. 6 (2021) 3261–3269, https://doi.org/10.1021/acsenergylett.1c01395.
[19] S.Y. Han, et al., Joule 5 (2021) 2450–2465, https://doi.org/10.1016/j.joule.2021.07.002.
[20] M. Jäckle, et al., Energy Environ. Sci. 11 (2018) 3400–3407, https://doi.org/10.1039/c8ee01448e.
[21] S. Kim, et al., Adv. Energy Mater. 10 (2020) 1903993, https://doi.org/10.1002/aenm.201903993.
[22] T. Krauskopf, et al., Chem. Rev. 120 (2020) 7745–7794, https://doi.org/10.1021/acs.chemrev.0c00431.
[23] K.N. Wood, et al., Nat. Commun. 9 (2018) 2490, https://doi.org/10.1038/s41467-018-04762-z.
[24] W. Zhao, et al., ACS Nano (2025), https://doi.org/10.1021/acsnano.4c14322.
[25] S. Bai, et al., Adv. Energy Mater. 13 (2023) 2301041, https://doi.org/10.1002/aenm.202301041.
[26] G. Li, et al., Energy Mater. 2 (2022) 200020, https://doi.org/10.20517/energymater.2022.24.
[27] H. Liu, et al., Energy Storage Mater. 55 (2023) 244–263, https://doi.org/10.1016/j.ensm.2022.11.054.
[28] W. Cai, et al., Chem. Soc. Rev. 49 (2020) 3806–3833, https://doi.org/10.1039/c9cs00728h.
[29] O. Tamwattana, et al., ACS Energy Lett. 6 (2021) 4416–4425, https://doi.org/10.1021/acsenergylett.1c02224.
[30] W. Chen, et al., Adv. Mater. 32 (2020) 2002850, https://doi.org/10.1002/adma.202002850.
[31] H.H. Weldeyohannes, et al., J. Power Sources 506 (2021) 230204, https://doi.org/10.1016/j.jpowsour.2021.230204.
[32] J. Maier Angew, Chem. Int. Ed 52 (2013) 4998–5026, https://doi.org/10.1002/anie.201205569.
[33] T. Krauskopf, et al., Adv. Energy Mater. 10 (2020) 2000945, https://doi.org/10.1002/aenm.202000945.
[34] F.P. McGrogan, et al., Adv. Energy Mater. 7 (2017) 1602011, https://doi.org/10.1002/aenm.201602011.
[35] H. Huo, et al., Adv. Mater. 37 (2025) e2415006, https://doi.org/10.1002/adma.202415006.
[36] C. Li, et al., Adv. Mater. 37 (2025) 2416377, https://doi.org/10.1002/adma.202416377.
[37] T. Palaniselvam, et al., J. Phys. Chem. C 126 (2022) 13043–13052, https://doi.org/10.1021/acs.jpcc.2c04024.
[38] W. Yan, et al., Nat. Energy 8 (2023) 800–813, https://doi.org/10.1038/s41560-023-01279-8.
[39] D.H.S. Tan, et al., Science 373 (2021) 1494–1499, https://doi.org/10.1126/science.abg7217.
[40] Y.-G. Lee, et al., Nat. Energy 5 (2020) 299–308, https://doi.org/10.1038/s41560-020-0575-z.
[41] Y. Wang, et al., Energy Storage Mater. 19 (2019) 80–87, https://doi.org/10.1016/j.ensm.2019.02.029.
[42] S. Muy, et al., Energy Environ. Sci. 11 (2018) 850–859, https://doi.org/10.1039/c7ee03364h.
[43] A. Yulaev, et al., Nano Lett. 18 (2018) 1644–1650, https://doi.org/10.1021/acs.nanolett.7b04518.
[44] C.P. Yang, et al., Nat. Commun. 6 (2015) 8058, https://doi.org/10.1038/ncomms9058.
[45] Z. Wang, et al., Green Carbon 1 (2023) 193–209, https://doi.org/10.1016/j.greenca.2023.12.001.

[46] M.R. Palacín, et al., Science 351 (2016) 574, https://doi.org/10.1126/science.1253292.
[47] W. Xu, et al., Energy Environ. Sci. 7 (2014) 513–537, https://doi.org/10.1039/c3ee40795k.
[48] D. Lin, et al., Nano Lett. 17 (2017) 3731–3737, https://doi.org/10.1021/acs.nanolett.7b01020.
[49] N.W. Li, et al., Angew. Chem. Int. Ed. 57 (2018) 1505–1509, https://doi.org/10.1002/anie.201710806.
[50] M.-S. Balogun, et al., Carbon 98 (2016) 162–178, https://doi.org/10.1016/j.carbon.2015.09.091.
[51] E. Kazyak, et al., Adv. Energy Mater. 12 (2021) 2102618, https://doi.org/10.1002/aenm.202102618.
[52] Y. Huang, et al., Angew. Chem. Int. Ed. 132 (2020) 3728–3733, https://doi.org/10.1002/ange.201914417.
[53] S. Schweidler, et al., J. Phys. Chem. C 122 (2018) 8829–8835, https://doi.org/10.1021/acs.jpcc.8b01873.
[54] J. Duan, et al., Adv. Mater. 31 (2019) e1807243, https://doi.org/10.1002/adma.201807243.
[55] Y.H. Lee, et al., Joule (2024), https://doi.org/10.1016/j.joule.2024.08.011.
[56] H. Wu, et al., Nano Lett. 12 (2012) 904–909, https://doi.org/10.1021/nl203967r.
[57] S.C. Minseong Ko, Sookyung Jeong, Oh Pilgun, Jaephil Cho, ACS Nano 8 (2014) 8591, https://doi.org/10.1021/nn503294z.
[58] B. Hertzberg, et al., Electrochem. Commun. 13 (2011) 818–821, https://doi.org/10.1016/j.elecom.2011.05.011.
[59] C.S. Hong, et al., Extreme Mech. Lett. 40 (2020) 100907, https://doi.org/10.1016/j.eml.2020.100907.
[60] L.A. Berla, et al., J. Power Sources 273 (2015) 41–51, https://doi.org/10.1016/j.jpowsour.2014.09.073.
[61] J.E. Trevey, et al., ECS Solid State Lett. 13 (2010) A154, https://doi.org/10.1149/1.3479551.
[62] N.A. Dunlap, et al., J. Electrochem. Soc. 167 (2020) 060522, https://doi.org/10.1149/1945-7111/ab84fc.
[63] L. Peng, et al., Energy Environ. Mater. 6 (2022) 12308, https://doi.org/10.1002/eem2.12308.
[64] M.C. Bay, et al., Adv. Energy Mater. 10 (2019) 1902899, https://doi.org/10.1002/aenm.201902899.
[65] J. Tippens, et al., ACS Energy Lett. 4 (2019) 1475–1483, https://doi.org/10.1021/acsenergylett.9b00816.
[66] G. Sahu, et al., Energy Environ. Sci. 7 (2014) 1053–1058, https://doi.org/10.1039/c3ee43357a.
[67] B.S. Vishnugopi, et al., Adv. Energy Mater. 12 (2021) 2102825, https://doi.org/10.1002/aenm.202102825.
[68] V. Thangadurai, et al., J. Am. Chem. Soc. 86 (2004) 437–440, https://doi.org/10.1111/j.1151-2916.2003.tb03318.x.
[69] R. Murugan, et al., Angew. Chem. Int. Ed. 46 (2007) 7778–7781, https://doi.org/10.1002/anie.200701144.
[70] S. Xia, et al., Chem 5 (2019) 753–785, https://doi.org/10.1016/j.chempr.2018.11.013.
[71] S. Qin, et al., Appl. Phys. Lett. 112 (2018) 113901, https://doi.org/10.1063/1.5019179.
[72] W.D. Richards, et al., Chem. Mater. 28 (2015) 266–273, https://doi.org/10.1021/acs.chemmater.5b04082.
[73] C. Wang, et al., Acc. Mater. Res. 3 (2021) 21–32, https://doi.org/10.1021/accountsmr.1c00137.
[74] W. Xia, et al., Chem. Rev. 122 (2022) 3763–3819, https://doi.org/10.1021/acs.chemrev.1c00594.
[75] D. Ren, et al., eTransportation 18 (2023), https://doi.org/10.1016/j.etran.2023.100272.
[76] Y. Nikodimos, et al., ACS Energy Lett. 9 (2024) 1844–1852, https://doi.org/10.1021/acsenergylett.4c00500.
[77] H. Lee, et al., Adv. Mater. 31 (2019) 1900376, https://doi.org/10.1002/adma.201900376.
[78] F. Han, et al., Adv. Energy Mater. 6 (2016) 1501590, https://doi.org/10.1002/aenm.201501590.
[79] P. Lu, et al., Electrochem. Energy Rev. 5 (2022) 149, https://doi.org/10.1007/s41918-022-00149-3.
[80] Y. Nikodimos, et al., Energy Environ. Sci. 15 (2022) 991–1033, https://doi.org/10.1039/d1ee03032a.
[81] X.L. Fan, et al., Sci. Adv. 4 (2018) 9245, https://doi.org/10.1126/sciadv.aau9245.
[82] B. Hennequart, et al., ACS Energy Lett. (2024) 454–460, https://doi.org/10.1021/acsenergylett.3c02513.
[83] K. Tuo, et al., Electrochem. Energy Rev. 6 (2023) 17, https://doi.org/10.1007/s41918-023-00179-5.
[84] Y. Zhu, et al., Angew. Chem. Int. Ed. 59 (2020) 17472–17476, https://doi.org/10.1002/anie.202007621.
[85] X. Li, et al., Nano Lett. 20 (2020) 4384–4392, https://doi.org/10.1021/acs.nanolett.0c01156.
[86] S. Wang, et al., Adv. Funct. Mater. 32 (2021) 2108805, https://doi.org/10.1002/adfm.202108805.
[87] W. Li, et al., Energy Environ. Sci. (2025), https://doi.org/10.1039/d4ee04927f.
[88] W. Li, et al., Nat. Nanotechnol. 20 (2025) 265–275, https://doi.org/10.1038/s41565-024-01813-z.
[89] N. Tapia-Ruiz, et al., Nat. Commun. 11 (2020) 4492, https://doi.org/10.1038/s41467-020-17951-6.
[90] P. Hartwig, et al., Angew. Chem. Int. Ed. 19 (2003) 74–75, https://doi.org/10.1002/anie.198000741.
[91] V. Gulino, et al., ACS Appl. Energy Mater. 4 (2021) 1228–1236, https://doi.org/10.1021/acsaem.0c02525.
[92] T. Yu, et al., Chem. Rev. 125 (2025) 3595–3662, https://doi.org/10.1021/acs.chemrev.4c00894.
[93] M. Arrese-Igor, et al., ACS Energy Lett. 7 (2022) 1473–1480, https://doi.org/10.1021/acsenergylett.2c00488.
[94] K. He, et al., Angew. Chem. Int. Ed. 60 (2021) 12116–12123, https://doi.org/10.1002/anie.202103403.
[95] C. Wang, et al., ACS Energy Lett. 7 (2021) 410–416, https://doi.org/10.1021/acsenergylett.1c02261.
[96] T. Schuler, et al., Adv. Energy Mater. 10 (2019) 1903216, https://doi.org/10.1002/aenm.201903216.
[97] H. Huo, et al., Adv. Energy Mater. 9 (2019) 1804004, https://doi.org/10.1002/aenm.201804004.
[98] M. Zhang, et al., Adv. Energy Mater. 14 (2024) 2303932, https://doi.org/10.1002/aenm.202303932.
[99] X. Yang, et al., Energy Environ. Sci. 13 (2020) 1318–1325, https://doi.org/10.1039/d0ee00342e.
[100] K. Zhang, et al., Adv. Energy Mater. 12 (2022) 2200368, https://doi.org/10.1002/aenm.202200368.
[101] W. Li, et al., ACS Energy Lett. 8 (2023) 5128–5135, https://doi.org/10.1021/acsenergylett.3c01558.
[102] S. Huo, et al., InfoMat 5 (2023) 12394, https://doi.org/10.1002/inf2.12394.
[103] M. Walkowiak, et al., Electrochem. Commun. 9 (2007) 1558–1562, https://doi.org/10.1016/j.elecom.2007.02.019.
[104] R. Chen, et al., Chem. Rev. 120 (2020) 6820–6877, https://doi.org/10.1021/acs.chemrev.9b00268.
[105] Q. Gu, et al., Acta Chim. Sinica 82 (2024) 449–457, https://doi.org/10.6023/A23120541.
[106] X. Shen, et al., Adv. Energy Mater. 11 (2021) 202003416, https://doi.org/10.1002/aenm.202003416.
[107] Z. Yu, et al., Adv. Energy Mater. 11 (2021) 2003250, https://doi.org/10.1002/aenm.202003250.
[108] J. Kang, et al., Energy Storage Mater. 52 (2022) 130–160, https://doi.org/10.1016/j.ensm.2022.07.037.
[109] Q. Zhang, et al., Adv. Mater. 31 (2019) 1901131, https://doi.org/10.1002/adma.201901131.
[110] S. Wang, et al., Angew. Chem. Int. Ed. 58 (2019) 8039–8043, https://doi.org/10.1002/anie.201901938.
[111] W. Li, et al., Adv. Mater. 36 (2024) 2302647, https://doi.org/10.1002/adma.202302647.
[112] K.J. Kim, et al., Adv. Energy Mater. 11 (2020) 2002689, https://doi.org/10.1002/aenm.202002689.
[113] L. Wang, et al., eTransportation 16 (2023), https://doi.org/10.1016/j.etran.2023.100239.
[114] F. Han, et al., Adv. Energy Mater. 8 (2018) 1703644, https://doi.org/10.1002/aenm.201703644.
[115] S. Deng, et al., ACS Energy Lett. 5 (2020) 1243–1251, https://doi.org/10.1021/acsenergylett.0c00256.
[116] X.B. Cheng, et al., Chem. Rev. 117 (2017) 10403–10473, https://doi.org/10.1021/acs.chemrev.7b00115.
[117] H. Koshikawa, et al., J. Power Sources 376 (2018) 147–151, https://doi.org/10.1016/j.jpowsour.2017.11.082.
[118] D. Lin, et al., Nat. Nanotechnol. 12 (2017) 194–206, https://doi.org/10.1038/nnano.2017.16.
[119] P. Albertus, et al., ACS Energy Lett. (2021) 1399–1404, https://doi.org/10.1021/acsenergylett.1c00445.
[120] Y. Peng, et al., Mater. Chem. Front. 8 (2024) 1421–1450, https://doi.org/10.1039/d3qm01023f.
[121] L. Ye, et al., Nat. Mater. 23 (2024) 244–251, https://doi.org/10.1038/s41563-023-01722-x.
[122] J.A. Lewis, et al., Nat. Mater. 20 (2021) 503–510, https://doi.org/10.1038/s41563-020-00903-2.
[123] Z. Wang, et al., Nat. Energy 9 (2024) 251–262, https://doi.org/10.1038/s41560-023-01426-1.
[124] J. Kasemchainan, et al., Nat. Mater. 18 (2019) 1105–1111, https://doi.org/10.1038/s41563-019-0438-9.
[125] Y. Su, et al., Energy Environ. Sci. 13 (2020) 908–916, https://doi.org/10.1039/c9ee04007b.
[126] N.W. Li, et al., Adv. Mater. 28 (2016) 1853–1858, https://doi.org/10.1002/adma.201504526.
[127] Y. Liu, et al., Nat. Commun. 7 (2016) 10992, https://doi.org/10.1038/ncomms10992.
[128] T. Krauskopf, et al., Adv. Energy Mater. 9 (2019) 1902568, https://doi.org/10.1002/aenm.201902568.
[129] S. Chen, et al., Adv. Mater. 30 (2018) 1706102, https://doi.org/10.1002/adma.201706102.
[130] R. Koerver, et al., Energy Environ. Sci. 11 (2018) 2142–2158, https://doi.org/10.1039/c8ee00907d.
[131] L. Zhao, et al., Adv. Energy Mater. 13 (2023), https://doi.org/10.1002/aenm.202300679.
[132] J. Electrochem, Soc 2 (2019) 166, https://doi.org/10.1149/2.0221902jes].
[133] Y. Liu, et al., Adv. Energy Mater. 12 (2022) 2103589, https://doi.org/10.1002/aenm.202103589.

[134] L. Braks, et al., Angew. Chem. Int. Ed. 63 (2024) e202408238, https://doi.org/10.1002/anie.202408238.
[135] O. Sheng, et al., Nano Lett. 22 (2022) 8346–8354, https://doi.org/10.1021/acs.nanolett.2c03291.
[136] N.G. Yadav, et al., J. Mater. Chem. A 10 (2022) 17142–17155, https://doi.org/10.1039/d2ta01889f.
[137] J. Liang, et al., Nat. Commun. 14 (2023) 146, https://doi.org/10.1038/s41467-022-35667-7.
[138] B. Li, et al., ACS Appl. Mater. Interfaces 14 (2022) 37738–37746, https://doi.org/10.1021/acsami.2c09013.
[139] H. Zhong, et al., Electrochim. Acta 277 (2018) 268–275, https://doi.org/10.1016/j.electacta.2018.04.191.
[140] K. Nie, et al., ACS Energy Lett. 5 (2020) 826–832, https://doi.org/10.1021/acsenergylett.9b02739.
[141] C. Jiang, et al., ACS Appl. Energy Mater. 7 (2024) 7110–7117, https://doi.org/10.1021/acsaem.4c01516.
[142] M. Li, et al., ACS Appl. Mater. Interfaces 13 (2021) 50076–50082, https://doi.org/10.1021/acsami.1c16356.
[143] Y. Zhang, et al., Chem. Eng. J. 461 (2023) 141993, https://doi.org/10.1016/j.cej.2023.141993.
[144] N. Delaporte, et al., Batteries Supercaps 5 (2022), https://doi.org/10.1002/batt.202200245.
[145] H.J. Choi, et al., Adv. Sci. 9 (2022) e2103826, https://doi.org/10.1002/advs.202103826.
[146] G.H. Lee, et al., J. Mater. Chem. A 10 (2022) 10662–10671, https://doi.org/10.1039/d1ta11066g.
[147] A. Wang, et al., Energy Storage Mater. 49 (2022) 246–254, https://doi.org/10.1016/j.ensm.2022.04.023.
[148] Z. Chen, et al., Adv. Energy Mater. 11 (2021) 2101339, https://doi.org/10.1002/aenm.202101339.
[149] J. Liang, et al., Adv. Energy Mater. 9 (2019) 1902125, https://doi.org/10.1002/aenm.201902125.
[150] Y. Gao, et al., Angew. Chem. Int. Ed. 57 (2018) 13608–13612, https://doi.org/10.1002/anie.201807304.
[151] H. Park, et al., Adv. Sci. 8 (2021) 2004204, https://doi.org/10.1002/advs.202004204.
[152] Y.N. Li, et al., Energy Storage Mater. 38 (2021) 262–275, https://doi.org/10.1016/j.ensm.2021.03.016.
[153] K. Fu, et al., Energy Environ. Sci. 10 (2017) 1568–1575, https://doi.org/10.1039/c7ee01004d.
[154] H. Duan, et al., Adv. Energy Mater. 13 (2023), https://doi.org/10.1002/aenm.202300815.
[155] K. Wang, et al., J. Mater. Sci. Technol. 153 (2023) 32–40, https://doi.org/10.1016/j.jmst.2022.12.055.
[156] X. Yang, et al., Energy Storage Mater. 27 (2020) 198–204, https://doi.org/10.1016/j.ensm.2020.01.031.
[157] Y. Peng, et al., Adv. Colloid Interface Sci. 307 (2022) 102732, https://doi.org/10.1016/j.cis.2022.102732.
[158] T.S. Wang, et al., Adv. Funct. Mater. 31 (2020) 2001973, https://doi.org/10.1002/adfm.202001973.
[159] S.S. Chi, et al., Energy Storage Mater. 17 (2019) 309–316, https://doi.org/10.1016/j.ensm.2018.07.004.
[160] Y. Chen, et al., ACS Appl. Mater. Interfaces 13 (2021) 28398–28404, https://doi.org/10.1021/acsami.1c07761.
[161] J. Wen, et al., Energy Storage Mater. 45 (2022) 934–940, https://doi.org/10.1016/j.ensm.2021.12.033.
[162] S. Nanda, et al., Adv. Energy Mater. 8 (2018) 1801556, https://doi.org/10.1002/aenm.201801556.
[163] J. Oh, et al., ACS Energy Lett. 7 (2022) 1374–1382, https://doi.org/10.1021/acsenergylett.2c00461.
[164] S. Nanda, et al., Adv. Energy Mater. 11 (2020) 2000804, https://doi.org/10.1002/aenm.202000804.
[165] H. Kwon, et al., Nat. Commun. 12 (2021) 5537, https://doi.org/10.1038/s41467-021-25848-1.
[166] L. Lin, et al., Adv. Energy Mater. 11 (2021) 2003709, https://doi.org/10.1002/aenm.202003709.
[167] W.Z. Huang, et al., Adv. Energy Mater. 12 (2022) 2201044, https://doi.org/10.1002/aenm.202201044.
[168] D. Spencer Jolly, et al., Joule 7 (2023) 503–514, https://doi.org/10.1016/j.joule.2023.02.001.
[169] J. Wen, et al., Adv. Mater. 36 (2024) e2307732, https://doi.org/10.1002/adma.202307732.
[170] K.H. Kim, et al., Nat. Commun. 15 (2024) 3586, https://doi.org/10.1038/s41467-024-48021-w.
[171] S.E. Sandoval, et al., Joule 7 (2023) 2054–2073, https://doi.org/10.1016/j.joule.2023.07.022.
[172] D. Jun, et al., Adv. Funct. Mater. (2023), https://doi.org/10.1002/adfm.202310259.
[173] J. Lee, et al., Adv. Mater. 34 (2022) e2203580, https://doi.org/10.1002/adma.202203580.
[174] T. Fuchs, et al., Nat. Mater. (2024), https://doi.org/10.1038/s41563-024-02006-8.
[175] G. Deysher, et al., Nat. Energy (2024), https://doi.org/10.1038/s41560-024-01569-9.
[176] L. Yuan, et al., Adv. Energy Mater. 14 (2024), https://doi.org/10.1002/aenm.202400125.
[177] Y. Ji, et al., Adv. Mater. 36 (2024) 2312548, https://doi.org/10.1002/adma.202312548.
[178] Z. Song, et al., Chem. Eng. J. 470 (2023) 144237, https://doi.org/10.1016/j.cej.2023.144237.
[179] Z. Song, et al., Adv. Energy Mater. 14 (2024), https://doi.org/10.1002/aenm.202401763.
[180] A. Schiele, et al., ACS Omega 3 (2018) 16706–16713, https://doi.org/10.1021/acsomega.8b02541.
[181] S.K. Heiskanen, et al., Joule 3 (2019) 2322–2333, https://doi.org/10.1016/j.joule.2019.08.018.
[182] Z. Zhang, et al., Energy Storage Mater. 54 (2023) 845–853, https://doi.org/10.1016/j.ensm.2022.11.023.
[183] C. Wang, et al., Angew. Chem. Int. Ed. 63 (2024) 202402301, https://doi.org/10.1002/anie.202402301.
[184] P. Peljo, et al., Energy Environ. Sci. 11 (2018) 2306–2309, https://doi.org/10.1039/c8ee01286e.
[185] S. Yang, et al., ACS Appl. Energy Mater. 5 (2021) 667–673, https://doi.org/10.1021/acsaem.1c03166.
[186] N. Zhang, et al., Batteries Supercaps 7 (2023) 202300488, https://doi.org/10.1002/batt.202300488.
[187] M.H. Kim, et al., ACS Energy Lett. 8 (2023) 3962–3970, https://doi.org/10.1021/acsenergylett.3c01134.
[188] N. Suzuki, et al., Adv. Energy and Sust. Res. 2 (2021) 2100066, https://doi.org/10.1002/aesr.202100066.
[189] J. Li, et al., Acta Mater. 244 (2023) 118592, https://doi.org/10.1016/j.actamat.2022.118592.
[190] Z. Wang, et al., Adv. Mater. (2023) 2310395, https://doi.org/10.1002/adma.202310395.
[191] M. Yang, et al., Adv. Energy Mater. 14 (2024) 2303229, https://doi.org/10.1002/aenm.202303229.
[192] X. Xing, et al., ACS Energy Lett. 6 (2021) 1831–1838, https://doi.org/10.1021/acsenergylett.1c00627.
[193] H. Zhang, et al., Energy Storage Mater. 36 (2021) 147–170, https://doi.org/10.1016/j.ensm.2020.12.027.
[194] D. Wei, et al., J. Mater. Chem. A 1 (2013) 3177, https://doi.org/10.1039/c3ta01183f.
[195] L.M. Bloi, et al., Carbon 188 (2022) 325–335, https://doi.org/10.1016/j.carbon.2021.11.061.
[196] W. Ping, et al., Energy Storage Mater. 21 (2019) 246–252, https://doi.org/10.1016/j.ensm.2019.06.024.
[197] B.T. Heligman, et al., ACS Energy Lett. 6 (2021) 2666–2672, https://doi.org/10.1021/acsenergylett.1c01145.
[198] W.M. Zhang, et al., Adv. Mater. 20 (2008) 1160–1165, https://doi.org/10.1002/adma.200701364.
[199] Y. Ma, et al., Nano Energy 42 (2017) 341–352, https://doi.org/10.1016/j.nanoen.2017.11.030.
[200] M.T. McDowell, et al., Adv. Mater. 24 (2012) 6034–6041, https://doi.org/10.1002/adma.201202744.
[201] Y. Peng, et al., Nano Energy 130 (2024) 110077, https://doi.org/10.1016/j.nanoen.2024.110077.
[202] S. Li, et al., Nat. Commun. 6 (2015) 7872, https://doi.org/10.1038/ncomms8872.
[203] J.S. Corsi, et al., ACS Energy Lett. 6 (2021) 1749–1756, https://doi.org/10.1021/acsenergylett.1c00324.
[204] W.J. Jeong, et al., ACS Energy Lett. 9 (2024) 2554–2563, https://doi.org/10.1021/acsenergylett.4c00915.
[205] S.Y. Han, et al., Chem. Mater. 32 (2020) 2461–2469, https://doi.org/10.1021/acs.chemmater.9b04992.
[206] S. Yanev, et al., J. Electrochem. Soc. 171 (2024) 020512, https://doi.org/10.1149/1945-7111/ad2594.
[207] J. Wan, et al., J. Am. Chem. Soc. 143 (2021) 839–848, https://doi.org/10.1021/jacs.0c10121.
[208] Y. Lu, et al., Sci. Adv. 7 (2021) 5520, https://doi.org/10.1126/sciadv.abi5520.
[209] M.N. Obrovac, et al., Chem. Rev. 114 (2014) 11444–11502, https://doi.org/10.1021/cr500207g.
[210] C. Cao, et al., Joule 3 (2019) 762–781, https://doi.org/10.1016/j.joule.2018.12.013.
[211] I. Na, et al., ACS Energy Lett. 8 (2023) 1936–1943, https://doi.org/10.1021/acsenergylett.3c00496.
[212] A. Song, et al., Adv. Energy Mater. 13 (2023) 2301464, https://doi.org/10.1002/aenm.202301464.
[213] Q. Huang, et al., Nat. Commun. 10 (2019) 5586, https://doi.org/10.1038/s41467-019-13434-5.
[214] R.B. Cervera, et al., Energy Environ. Sci. 7 (2014) 662–666, https://doi.org/10.1039/c3ee43306d.
[215] Y. Xin, et al., Adv. Funct. Mater. (2024) 2403222, https://doi.org/10.1002/adfm.202403222.
[216] S. Cangaz, et al., Adv. Energy Mater. 10 (2020) 2001320, https://doi.org/10.1002/aenm.202001320.
[217] Z. Wan, et al., J. Power Sources 505 (2021) 230062, https://doi.org/10.1016/j.jpowsour.2021.230062.
[218] S. An, et al., Adv. Energy Sustain. Res. 4 (2023) 2300092, https://doi.org/10.1002/aesr.202300092.
[219] H.W. Park, et al., Jpn. J. Appl. Phys. 53 (2014) 08NK02, https://doi.org/10.7567/jjap.53.08nk02.

[220] L. Zhang, et al., ACS Appl. Mater. Interfaces 14 (2022) 24798–24805, https://doi.org/10.1021/acsami.2c04487.
[221] S.Y. Ham, et al., Nat. Commun. 15 (2024) 2991, https://doi.org/10.1038/s41467-024-47352-y.
[222] G. Zhu, et al., Angew. Chem. Int. Ed. 58 (2019) 6669–6673, https://doi.org/10.1002/anie.201902083.
[223] J. Lee, et al., Adv. Energy Mater. 13 (2023) 2300172, https://doi.org/10.1002/aenm.202300172.
[224] J. Kim, et al., J. Power Sources 510 (2021) 230425, https://doi.org/10.1016/j.jpowsour.2021.230425.
[225] N.A. Dunlap, et al., Solid State Ion. 324 (2018) 207–217, https://doi.org/10.1016/j.ssi.2018.07.013.
[226] M. Kim, et al., Adv. Sci. 10 (2023) e2301381, https://doi.org/10.1002/advs.202301381.
[227] Z. Zhang, et al., Energy Environ. Sci. 17 (2024) 1061–1072, https://doi.org/10.1039/d3ee03877g.
[228] T.A. Yersak, et al., J. Electrochem. Soc. 160 (2013), https://doi.org/10.1149/2.086309jes].
[229] F. Mo, et al., ACS Appl. Mater. Interfaces 12 (2020) 38232–38240, https://doi.org/10.1021/acsami.0c11001.
[230] C. Yang, et al., Adv. Mater. 31 (2018) 1804815, https://doi.org/10.1002/adma.201804815.
[231] X. He, et al., ACS Energy Lett. 7 (2021) 131–139, https://doi.org/10.1021/acsenergylett.1c02122.
[232] E. Zhou, et al., J. Am. Chem. Soc. 146 (2024) 20700–20708, https://doi.org/10.1021/jacs.4c03680.
[233] H. Sun, et al., J. Power Sources 597 (2024) 234118, https://doi.org/10.1016/j.jpowsour.2024.234118.
[234] Z. Wang, et al., eScience 3 (2023), https://doi.org/10.1016/j.esci.2022.100087.
[235] C. Hänsel, et al., Chem. Mater. 33 (2021) 6029–6040, https://doi.org/10.1021/acs.chemmater.1c01431.
[236] X. Gao, et al., Adv. Funct. Mater. 33 (2022), https://doi.org/10.1002/adfm.202209715.
[237] G. Ferraresi, et al., ACS Energy Lett. 3 (2018) 1006–1012, https://doi.org/10.1021/acsenergylett.8b00264.
[238] X. Xu, et al., Small 19 (2023) 2302934, https://doi.org/10.1002/smll.202302934.
[239] Z. Li, et al., Chem. Eng. J. 465 (2023) 142895, https://doi.org/10.1016/j.cej.2023.142895.
[240] Y. Cheng, et al., Angew. Chem. Int. Ed. 62 (2023) 05723, https://doi.org/10.1002/anie.202305723.
[241] Z. Song, et al., J. Power Sources 640 (2025) 236798, https://doi.org/10.1016/j.jpowsour.2025.236798.
[242] J.Y. Kim, et al., Adv. Energy Mater. 12 (2021) 2103108, https://doi.org/10.1002/aenm.202103108.
[243] C. Wang, et al., Chem. Rev. 120 (2020) 4257–4300, https://doi.org/10.1021/acs.chemrev.9b00427.
[244] Y. Liu, et al., Nat. Commun. 14 (2023) 3975, https://doi.org/10.1038/s41467-023-39685-x.